Chinese Journal of Chemical Engineering 89 (2026) 334–352

Contents lists available at ScienceDirect

Chinese Journal of Chemical Engineering

journal homepage: www.elsevier.com/locate/CJChE

Full Length Article

Novel intensification strategy for the liquid-only transfer dividing wall column separating ternary mixtures based on the column grand composite curve

Zhongwen Song [1], Chenghao Xing [2], Yanyang Wu [2,*], Guilian Liu [1,*]

[1] School of Chemical Engineering and Technology, Xi'an Jiaotong University, Xi'an 710049, China
[2] School of Chemical Engineering, East China University of Science & Technology, Shanghai 200237, China

ARTICLE INFO

Article history:
Received 12 May 2025
Received in revised form
26 July 2025
Accepted 27 July 2025
Available online 28 October 2025

Keywords:
Dividing wall column
Intensification
Vapor recompression
Intermediate reboiler
Optimization

ABSTRACT

The liquid-only transfer dividing wall column (LDWC) offers a promising path for industrializing dividing wall columns by simplifying vapor split control. However, their energy efficiency is insufficient due to the addition of heat at the bottom and its removal at the top. Therefore, developing an effective strategy to enhance the energy efficiency of the entire LDWC system is crucial. This work investigates the intensification of LDWC based on the column grand composite curve (CGCC) and thermodynamic analysis, proposing a novel intensification strategy to improve energy efficiency effectively. An optimization model with four blocks is developed to minimize the total annual cost (TAC) of the intensified LDWC. Energy, exergy, economic, and environmental analyses are used to evaluate its performance. Ternary mixtures with different easy separation indexes (ESI) are selected as illustrative examples. For mixtures with ESI $\leq$1, the optimal configuration involves partial feed preheating, compressors and intermediate reboilers on both side sections, along with optimized operating pressure. This setup leads to significant reductions in total energy consumption, TAC, and gas emissions by 43.80%, 28.08%, and 42.85% for ESI = 1, and by 46.17%, 29.06%, and 45.35% for ESI <1, respectively, when compared to conventional distillation sequences (CDS). For mixtures with ESI >1, the best performance is achieved by implementing partial feed preheating and modifications only to the right section. This results in reductions of 21.64% in energy consumption, 16.26% in TAC, and 21.51% in gas emissions when compared to CDS. In all cases, the optimal configurations show the lowest lost work and minimum work, indicating an improved thermodynamic performance.

1. Introduction

Distillation, a widely utilized separation technology for liquid mixtures [1], plays a critical role in the chemical industry, accounting for 5% to 15% of global energy consumption [2,3]. Over the past few decades, substantial research efforts have been dedicated to improving the energy efficiency of distillation processes. These endeavors have explored advanced techniques, including reactive distillation [4,5], pressure-swing distillation [6,7], membrane distillation [4,5], and thermally coupled distillation [6,7]. Among these, thermally coupled distillation has drawn considerable attention from both industry and academia due to its exceptional energy-saving potential.

A prominent example of thermally coupled distillation is the dividing wall column (DWC), first proposed by Wright in 1949 [8]. It features a vertical wall for reducing the back-mixing of the intermediate component, leading to approximately 20% savings in energy consumption [9] and total annual cost (TAC) [10] compared to conventional distillation sequences (CDS) for separating ternary mixtures. Despite these advantages, DWC has not yet become a primary choice in industrial applications due to the challenges associated with controlling the vapor split ratio [7], which is generally constrained in a narrow operating range [11]. A local disturbance, such as fluctuations in the liquid split ratio, may cause the vapor split to fall outside the desired range, resulting in increased total energy consumption and TAC required to produce

* Corresponding authors.
E-mail addresses: wyywitty@ecust.edu.cn (Y. Wu), guilianliui@mail.xjtu.edu.cn (G. Liu).

https://doi.org/10.1016/j.cjche.2025.07.021

the desired products. To address this issue, Agrawal [7] and Ramapriya *et al.* [12] developed a modified structure by expanding the corresponding column sections and adding a condenser and reboiler. In this column, the bi-directional vapor and liquid streams of DWC are converted into liquid-only streams, resulting in a new equivalent DWC known as the liquid-only transfer DWC (LDWC) [12] illustrated in Fig. 1. The shortcut methods based on the Underwood equation [13] or those that combine thermodynamic calculations with specific enthalpy [14] can be utilized to design the initial structure configurations of LDWC systems for separating multicomponent mixtures. This approach serves as a basis for further research on LDWC.

Several researchers have studied the steady-state performance of LDWC. Feng *et al.* [15] and Zhang *et al.* [16] established the LDWC module in the commercial software Aspen Plus using the RadFrac module, while the heat transfer of the wall is ignored. Wu *et al.* [17] investigated the LDWC for separating equimolar mixtures of 1,2-ethanediol, 1,3-propanediol, and 1,4-butanediol and optimized the structural parameters. Compared to CDS, the application of LDWC resulted in a 17% reduction in *TAC*, a 28% decrease in cooling utility consumption, and a 19% decrease in heating utility consumption. Cui *et al.* [18] designed ten distillation sequences for separating an equimolar mixture of benzene, toluene, and xylene. The dynamic differential evolution algorithm with the TAC as the objective function was employed to optimize the operating parameters. The results indicated that the LDWC can effectively reduce back-mixing of the intermediate component, requiring minimal energy and TAC. Therefore, LDWC provides a reassuring solution for the industry.

Besides the steady-state performance of LDWC, its dynamic control has also been studied. Cui *et al.* [19] studied the LDWC separating an equimolar mixture of benzene, toluene, and xylene. They developed a control scheme with seven concentration controllers to maintain product purity when the feed flow and composition have ±20% disturbances. A modified temperature control scheme with only one internal concentration controller was then implemented to avoid the expense of multiple concentration controllers. This scheme handled ±20% disturbances with the minimum integral absolute error (IAE). Liu *et al.* [20] implemented a temperature control scheme with seven temperature controllers to effectively handle a ±20% feed disturbance of the

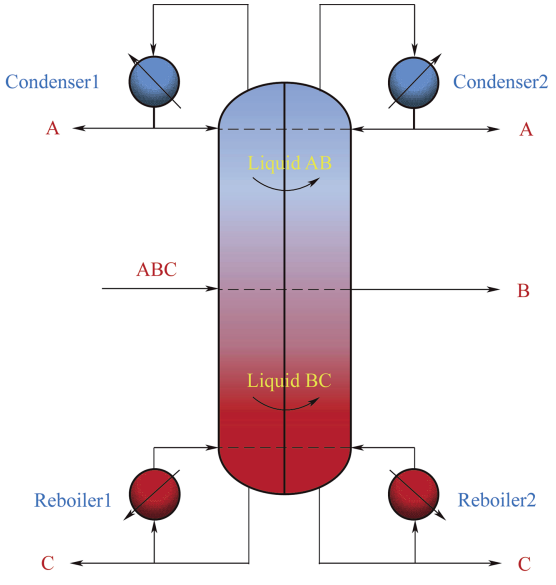

Fig. 1. LDWC structure diagram for separating a ternary mixture.

LDWC separating benzene-toluene-xylene mixtures. Kong *et al.* [21] investigated the dynamic control of LDWC for separating equimolar mixtures of benzene, toluene, xylene, and mesitylene. They found that a concentration control scheme with feedforward control could effectively handle feed disturbances of ±20%. A modified temperature control scheme with three concentration controls enables the system to handle feed disturbances of ±20% with a shorter response time, resulting in a lower IAE. Feng *et al.* [15], Zhang *et al.* [16], and Li *et al.* [22] studied the dynamic performance of the LDWC in separating multiple diol mixtures, demonstrating that the elemental concentration and temperature control schemes effectively handle feed disturbances. Based on the study introduced above, it can be observed that the LDWC exhibits excellent control performance, providing a solid foundation for its industrialization.

However, the energy efficiency of LDWC needs to be improved because all the heat is supplied at the bottom and removed from the top. Song *et al.* [23] proposed an intensified LDWC configuration with vapor recompression (VRC) technology employed to compress the side vapor product of the right column, providing heat for the intermediate reboiler (IR). The optimization results indicated that it can reduce energy consumption by 32.6% compared to CDS. The column grand composition curve (CGCC) [24], was used as the analysis tool in their study. Tututi-Avila *et al.* [25] coupled LDWC with extractive distillation, evolving the liquid-only transfer extractive dividing wall column (E-LDWC) to improve energy efficiency. For the separation of ethanol-water and acetone-methanol mixtures, the application of E-LDWC can reduce the total energy consumption by 13.5% and 14.3%, respectively, compared to traditional extractive distillation. Xing *et al.* [26] applied the E-LDWC to separate water-ethanol. The VRC technology was then used to compress the overheated vapor of the right column and provide heat for the IR. Based on this, the total energy consumption is reduced by 39% compared to conventional extractive distillation. The above studies demonstrate that E-LDWC is suitable for specific distillation processes, while VRC technology has a broader range of applications. Consequently, VRC technology is a more universal intensification method to utilize the energy of LDWC efficiently.

Based on the open literature survey, the LDWC solved the difficulty of controlling the vapor split ratio of DWC and has high energy efficiency and excellent dynamic control performance. Meanwhile, all the heat of the LDWC is supplied at the bottom and removed at the top, resulting the energy loss. Because of this, there is potential for reducing energy consumption and improving the energy efficiency of LDWC further through process intensification. However, no corresponding efficient strategy is reported.

This study aims to propose an effective intensification strategy combined with CGCC and thermodynamic analysis and identify the VRC intensification configuration to improve the energy efficiency of the entire LDWC system. A universal optimization model including four blocks will be designed to minimize TAC for the intensified LDWC through the sequence iterative approach. Ternary mixtures with different easy separation indexes (ESIs) are selected as illustrative examples, while energy, exergy, economic, and environmental analyses are used to evaluate their performance. This study can provide novel insight into the intensification of LDWC separating a ternary mixture.

2. Methodology

2.1. Problem statement

LDWC, as an improved DWC, can improve the energy efficiency of distillation and exhibit excellent stable and dynamic

performance [12]. For the separation of a ternary mixture, the structural configuration of the LDWC is illustrated in Fig. 1. The vertical dividing wall partitions the column into the left (CL) and right (CR) sections. In this arrangement, the light component (A) and part of the intermediate component (B) are extracted from the rectifying section of the CL and directed to the upper part of the CR for further separation. Simultaneously, the heavy component (C) and the remaining portion of the intermediate component (B) are extracted from the stripping section of the CL and fed into the lower part of the CR for sharp separation. Assuming no heat transfer across the dividing wall, the equivalent LDWC model for separating a ternary mixture is constructed using the RadFrac module in Aspen Plus, as shown in Fig. 2.

To maintain stable and continuous operation, high-quality energy is supplied at the bottom reboiler and removed from the top condenser of the LDWC, resulting the energy loss. Process intensification using advanced technology, such as VRC technology, offers a promising path to enhance the energy efficiency of distillation systems. However, there is a lack of an effective intensification strategy for the LDWC intensification using VRC technology. Therefore, developing an efficient intensification strategy tailored to the LDWC is essential for maximizing its energy efficiency.

Since the feed mixture characteristics strongly influence the performance of distillation processes, it is crucial to analyze LDWC configurations with varying feed properties to devise an effective intensification strategy. The easy separation index (ESI), defined as the ratio of the relative volatility between adjacent components, serves as a valuable indicator of feed mixture characteristics [27]. Systems separating mixtures with different ESI values exhibit varying energy consumption and theoretical stages and, thus, different intensified configurations. For ternary mixtures, the ESI equals α_{AB}/α_{BC}, where A, B, and C represent the components in order of decreasing volatility, and α is the relative volatility. Based on this index, feed mixtures can be categorized into three types: the mixtures with ESI = 1, ESI<1, and ESI>1.

Three types of equimolar aromatic mixtures with different ESI values are selected to illustrate the quantitative analysis. They are benzene-toluene-*p*-xylene with ESI = 1 (BzTX, Case 1), benzene-toluene-mesitylene with ESI<1 (BzTM, Case 2), and benzene-*p*-xylene-mesitylene with ESI>1 (BzXM, Case 3). Their properties are listed in Table 1. The flow rate of each mixture is assumed to be 300 kmol·h^{-1}, the target product purity is 99% (mol), the initial operating pressure of the LDWC is 101 kPa, and the pressure drop across the stages is neglected. Meanwhile, the feed inlet the system as a saturated liquid with temperatures of

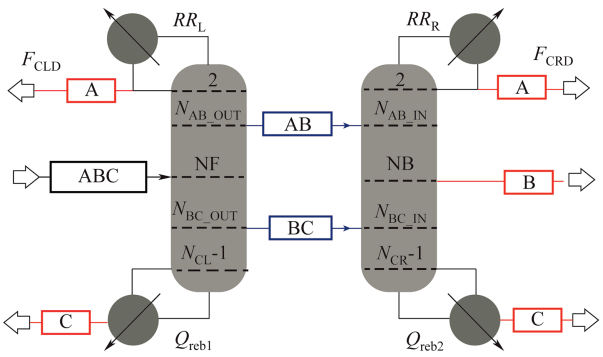

Fig. 2. The equivalent model of LDWC for separating a ternary mixture.

Table 1
The properties of selected mixtures.

Case	Mixtures	Normal boiling point /K	Relative volatility	ESI
Case 1	Benzene (Bz)	353	$\alpha_{BzT} = 2.39$	1.02
	Toluene (T)	384	$\alpha_{TX} = 2.34$	
	p-Xylene (X)	412		
Case 2	Benzene (Bz)	353	$\alpha_{BzT} = 2.39$	0.45
	Toluene (T)	384	$\alpha_{TM} = 5.28$	
	Mesitylene (M)	438		
Case 3	Benzene (Bz)	353	$\alpha_{BzX} = 5.21$	2.34
	p-Xylene(X)	412	$\alpha_{XM} = 2.22$	
	Mesitylene (M)	438		

376.0 K, 378.9 K, and 386.1 K for mixtures with ESI = 1, ESI <1, and ESI >1, respectively. The rigorous calculation is carried out in Aspen Plus V11.

2.2. Thermodynamic method

For the benzene-toluene, toluene-*p*-xylene, and benzene-*p*-xylene binary systems, the vapor-liquid equilibrium (VLE) data are obtained from the experiments conducted by Zhou *et al.* [28], Hu *et al.* [29], and Jin *et al.* [30], respectively. The non-random two-liquid (NRTL) model [31] is used to correlate the VLE data, which fits the experimental data well, as illustrated in Fig. S1 in the Supplementary Material. Thus, NRTL is selected as the thermodynamic method for this study. The missed binary interaction parameters can be estimated using the UNIFAC method [32]. The corrected binary interaction parameters are shown in Table S1.

2.3. Evaluation of LDWC

The performance of LDWC can be evaluated based on the energy, exergy, economic, and environmental analysis.

2.3.1. Energy analysis

In the energy analysis, the total energy consumption (Q_E) can be calculated from Eq. (1) [33].

$$Q_E = Q_R + c\sum W_n \tag{1}$$

where Q_R (kW) represents the total heat duty of all heaters; W_n (kW) represents the electricity requirement of unit n; c is the conversion coefficient of electricity to heat, which is set as 3 [34].

2.3.2. Exergy analysis

Exergy represents the maximum theoretical work required to transition a system from its initial state to thermodynamic equilibrium with an infinite reference environment [35]. Exergy analysis can quantitatively evaluate energy loss and guide energy-saving retrofits [36]. In such analyses, exergy/work loss (LW) and minimum work (W_{min}) are commonly employed as key evaluation metrics. For the continuous and stable system, they can be calculated according to Eqs. (2) and (3), respectively [37].

$$\begin{aligned} LW = &\sum\left[\frac{m(H-T_0S)}{3600}\right]_{in} - \sum\left[\frac{m(H-T_0S)}{3600}\right]_{out} + \sum W_{in} \\ &- \sum W_{out} + \sum\left[Q\left(1-\frac{T_0}{T}\right)\right]_{in} \\ &- \sum\left[Q\left(1-\frac{T_0}{T}\right)\right]_{out} \end{aligned} \tag{2}$$

$$W_{\min} = \sum \left[\frac{m(H - T_0 S)}{3600}\right]_{\text{out}} - \sum \left[\frac{m(H - T_0 S)}{3600}\right]_{\text{in}} \quad (3)$$

where m (kmol·h^{-1}), H (kJ·kmol^{-1}), and S (kJ·kmol^{-1}·K^{-1}) represent the molar flow rate, enthalpy, and entropy of the streams, respectively; subscripts "in" and "out" denote inlet and outlet of the system; W represents the work done to the system (W_{in}) or the surrounding (W_{out}); Q (kW) is the heat duty of the reboiler or condenser; T (K) is the temperature of the heat source or sink; T_0 (K) is the environment temperature.

2.3.3. Economic analysis

The total annual cost (TAC) is used as the evaluation index for economic analysis, comprising mainly operating and capital costs, as defined in Eq. (4) [38].

$$\text{TAC}\left(\text{USD}\cdot\text{a}^{-1}\right) = \text{Operating cost (OC)} + \frac{\text{Capital cost (CC)}}{\text{Payback year}} \quad (4)$$

where the operating cost (OC) comprises the expenses for hot and cold utilities, as well as electricity. Cooling water is used as the cold utility, priced at 0.354 USD·GJ^{-1} [39]. High-temperature steams are used as hot utilities; their prices are shown in Table 2 [23]. The cost of electricity is 0.10 USD·(kW·h)$^{-1}$ [40]. The capital cost (CC) includes equipment purchase and installation costs, such as shells, trays, heat exchangers, and compressors, and are calculated based on References [23,38], as shown in Table 3. All equipment is assumed to be made of carbon steel, and the Marshall & Swift index (M&S) of 2018, 1638.2 [41], will be used. The logarithmic mean temperature difference is set around 10 K for heat exchangers [23,26]. The maximum payback time is assumed to be 10 years [42].

2.3.4. Environmental analysis

The steam consumed by heaters is usually generated based on coal combustion in the Chinese industrial system, which discharges some gas pollutants, such as CO_2, SO_2, and NO_x [43]. Therefore, the gas emissions (G_{emission}, t·a^{-1}) are used for environmental analysis and can be calculated by eq (5) [44]. Equivalent coal (M_{coal}, t·a^{-1}) and electricity (W_{elec}, kW·h^{-1}·a^{-1}) consumption are identified based on Eqs. (6) and (7) [40].

$$G_{\text{emission}} = \sum_i \left(a_i M_{\text{coal}} + \frac{b_i W_{\text{elec}}}{1000}\right) \quad (5)$$

$$M_{\text{coal}} = 3.6 \cdot \frac{Q_{\text{R}} t}{Q_{\text{st}}} \quad (6)$$

$$W_{\text{elec}} = W_n t \quad (7)$$

where the subscript i denotes the type of gas; a and b are the emission conversion factors of equivalent coal and electricity, as shown in Table 4; Q_{st} is the calorific value of standard coal, 29307.6 kJ·kg^{-1}; t represents the annual operating time, and is taken as 8000 h·a^{-1} in this study.

3. Process Intensification

A conventional distillation column with one feed and two products is widely used in industry due to its simple structure and stable control [36] and will be used as the base case in this study. Its energy efficiency is low due to the back-mixing of the intermediate component.

3.1. Thermodynamic analysis of LDWC

Thermodynamic analysis of LDWC helps understand its operational characteristics and guides its intensification. Based on the feed and product locations, the LDWC for separating a ternary mixture is divided into eight sections, as illustrated in Fig. 3(a). The subsystems comprising CL_{mid1} and CL_{mid2}, CR_{top} and CR_{mid1}, or CR_{mid2} and CR_{bot} can be taken as conventional distillation columns with one feed and two product streams. The sections above the feed, including CL_{mid1}, CR_{top}, CR_{mid2}, and CL_{top}, are approximated as rectifying sections, which typically have excess heat and are considered potential heat sources (red areas) [45]. The sections below the feed, including CL_{mid2}, CR_{mid1}, CR_{bot}, and CL_{bot}, are approximated as stripping sections, which usually consume heat

Table 2
The price of high-temperature steams.

Case	Pressure /kPa	Latent heat /kJ·kg^{-1}	Temperature /K	Price /USD·GJ^{-1}
Case 1	451	2119.83	421	7.23
	671	2071.16	436	7.45
Case 2	541	2098.39	428	7.33
	1221	1982.33	462	7.85
Case 3	881	2033.39	448	7.62
	1231	1980.96	462	7.86

Table 4
The conversion factors for emission gases.

i	CO_2	SO_2	NO_X
a /kg·kg^{-1}	2.493	0.075	0.0375
b /kg·kW^{-1}·h^{-1}	0.997	0.030	0.015

Table 3
The details of TACs calculation.

Capital cost (CC)/USD		
	Shell/USD	$\frac{\text{M\&S}}{280} \times 937.636 \times D^{1.066} \times H_c^{0.802} \times (2.18 + F_c) \times \theta$ where H_c (m) $= (N_{\text{actual}} - 1) \times 0.6096 + 6$
	Tray/USD	$\frac{\text{M\&S}}{280} \times 97.243 \times D^{1.55} \times H_t \times F_c$ where H_t (m) $= (N_{\text{actual}} - 1) \times 0.6096$
	Heat exchanger /USD	$\frac{\text{M\&S}}{280} \times 474.668 \times A^{0.65} \times (2.29 + F_c)$ where A (m^2) $= \frac{Q}{U \cdot \Delta T}$
	Compressor/USD	$\frac{\text{M\&S}}{280} \times 517.5 \times \left(\frac{bhp}{0.7457}\right)^{0.82} \times (2.11 + F_c)$
Operating cost (OC)/USD·a^{-1}		
	Heating steam /USD·a^{-1}	$C_h \times Q_R \times 8000$
	Cooling water /USD·a^{-1}	$C_c \times Q_C \times 8000$
	Electricity /USD·a^{-1}	$C_e \times bhp \times 8000$

Note: the symbols' meanings are explained in Ref. [23].

and can be considered potential heat sinks (blue areas) [45]. Therefore, the LDWC has four potential heat sources and heat sinks for separating a ternary mixture, as shown in Fig. 3(b).

3.2. Intensification analysis based on the column grand composite curves

The column grand composite curves (CGCCs) obtained from the thermal analysis tools in the Aspen Plus can be plotted in the stage-enthalpy deficit (S-H) diagram. The enthalpy deficits represent the cumulative heating and cooling requirements for the column to operate at the practical near-minimum thermodynamic condition (PNMTC) approximation [46]. The inflection points on the S-H diagram may not coincide with the feed and extracted positions of LDWC due to the inevitable availability loss during separation. Combining the CGCCs with the potential heat source and heat sink ranges can guide the intensification of LDWC.

3.2.1. Separation of the BzTX mixture with ESI = 1

For the BzTX (benzene (Bz), toluene (T), *p*-xylene(X)) system, the relative volatilities of adjacent pairs of components are approximately equal, and ESI = 1. The S-H diagrams of LDWC, combined with the potential heat sources and heat sinks for separating the BzTX mixture, are shown in Fig. 4. The stage temperatures are indicated on the right *y*-axis.

Fig. 4(a) shows the combined S-H diagram for the CL section, including two potential heat sources and heat sinks. The heat sources span from stages 1 to 24, while the heat sinks span from stages 25 to 54. Heat source 2 has a small enthalpy deficit, while the middle position of the two heat sinks has a high enthalpy deficit. If the VRC technology is applied to extract the vapor stream

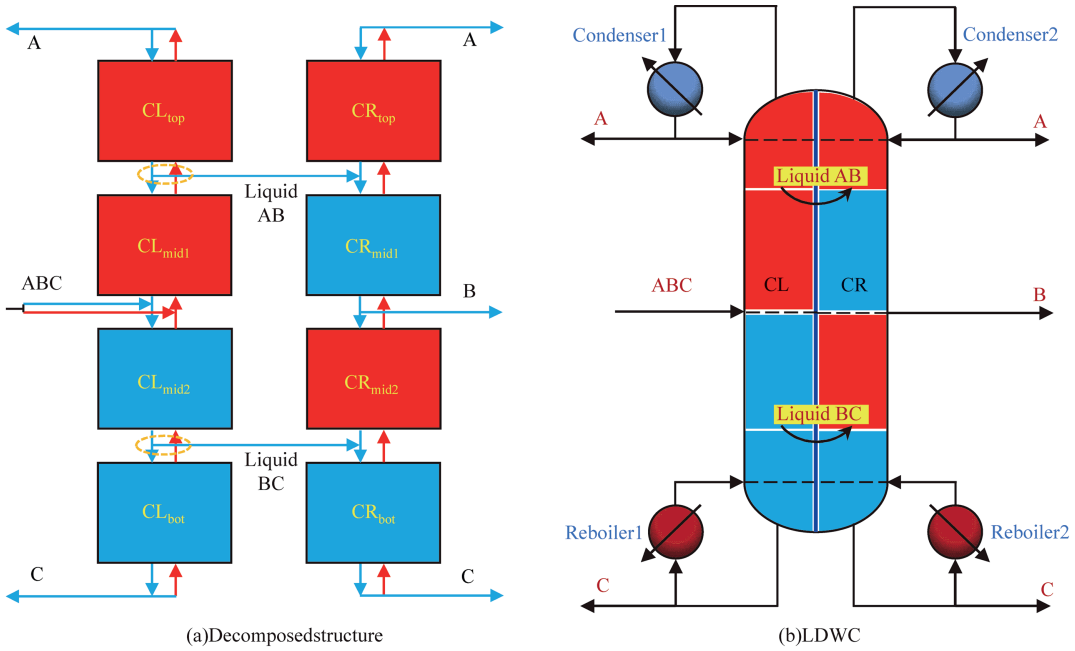

Fig. 3. Potential heat sources (red areas) and heat sinks (blue areas).

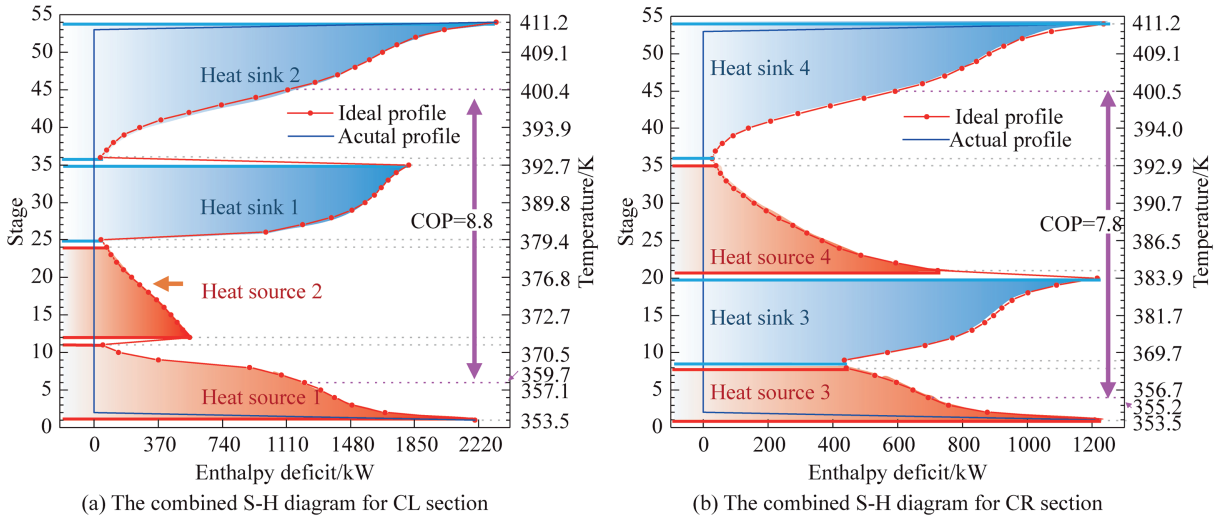

Fig. 4. The combined S-H diagrams for LDWC separating the BzTX mixture.

from heat source 2 and compress it by compressor to provide heat for the heat sinks through IR, a significant amount of electricity would be consumed, which could result in higher total energy consumption. Therefore, heat source 2 does not deserve to be recycled. Above heat sink 1, the enriched liquid is extracted and sent to CR, realizing the material and energy coupling between CL and CR and intensified internal operation. Since heat sink 1 is relatively narrow, its modification using VRC technology could disrupt material and energy coupling, thus increasing total energy consumption. Due to heat source 1 having a high enthalpy deficit and heat sink 2 having a relatively small enthalpy deficit in their middle position, their coefficient of performance (COP) exceeds 5 [26,47] (calculated as 359.7/(400.4−359.7) = 8.8). As a result, VRC technology can be used to compress the vapor stream of heat source 1 to provide heat for heat sink 2. Meanwhile, the mixture features a wide boiling range in this case. The bottom product stream can be used for preheating the feed to utilize heat effectively. Additionally, to minimize compressor power, the bottom stream can be further used to preheat the vapor stream extracted from the heat source 1.

Fig. 4 (b) shows the combined S-H diagram for the CR section, including two potential heat sources and heat sinks. The heat sources are mainly from stages 1 to 8 and stages 21 to 35, while the heat sinks are from stages 9 to 20 and stages 36 to 54. Due to the small enthalpy deficit in the middle of heat source 4, extracting and compressing the vapor from this section using VRC technology for heat recycling is not advisable. Meanwhile, the heat sink 3 lies between the side draw and the enriched liquid feed. Adding an IR into this area would result in a significant availability loss and increase total energy consumption. Therefore, modifying heat sink 3 is not recommended. Due to the

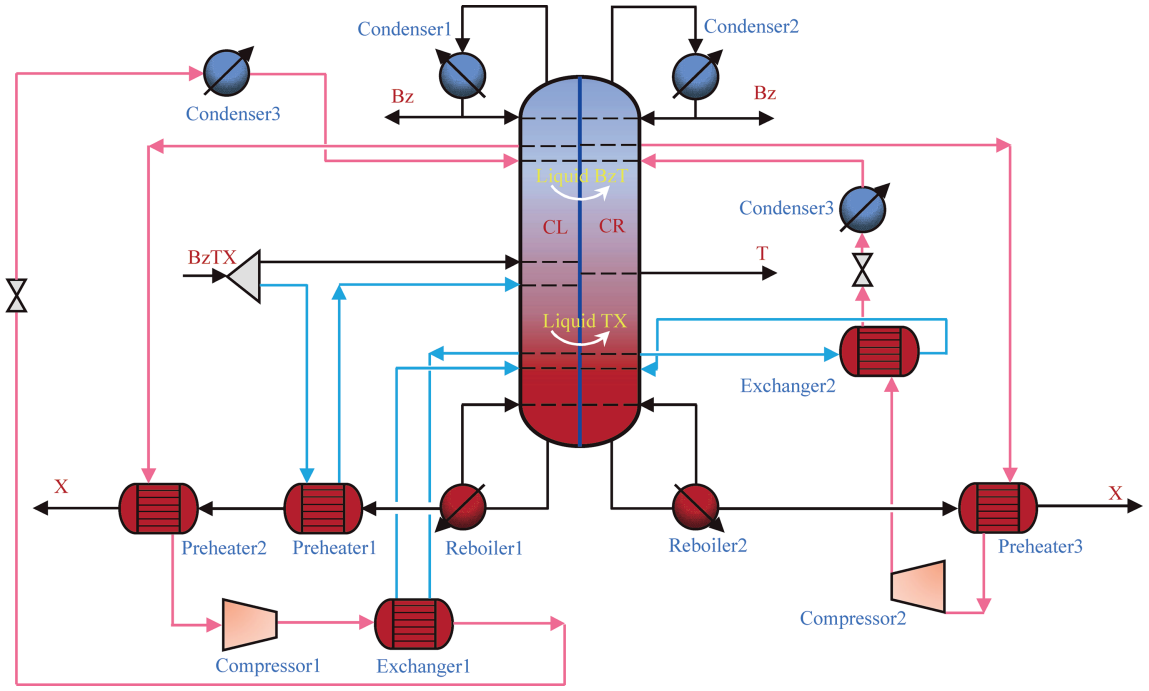

Fig. 5. Intensified LDWC structure for separating the BzTX mixture with ESI>1.

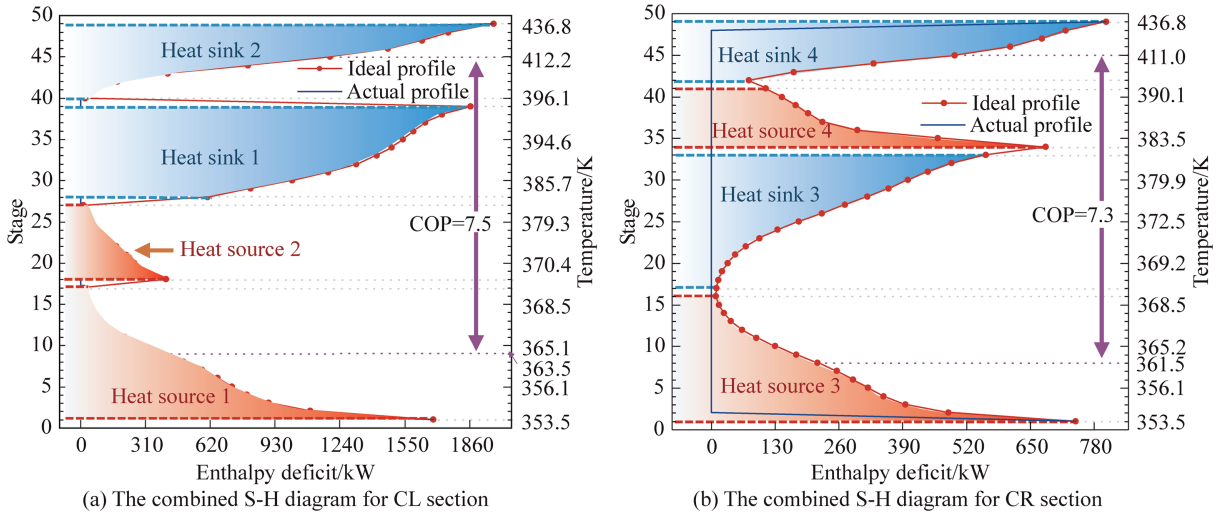

Fig. 6. The combined S-H diagrams for LDWC separating the BzTM mixture.

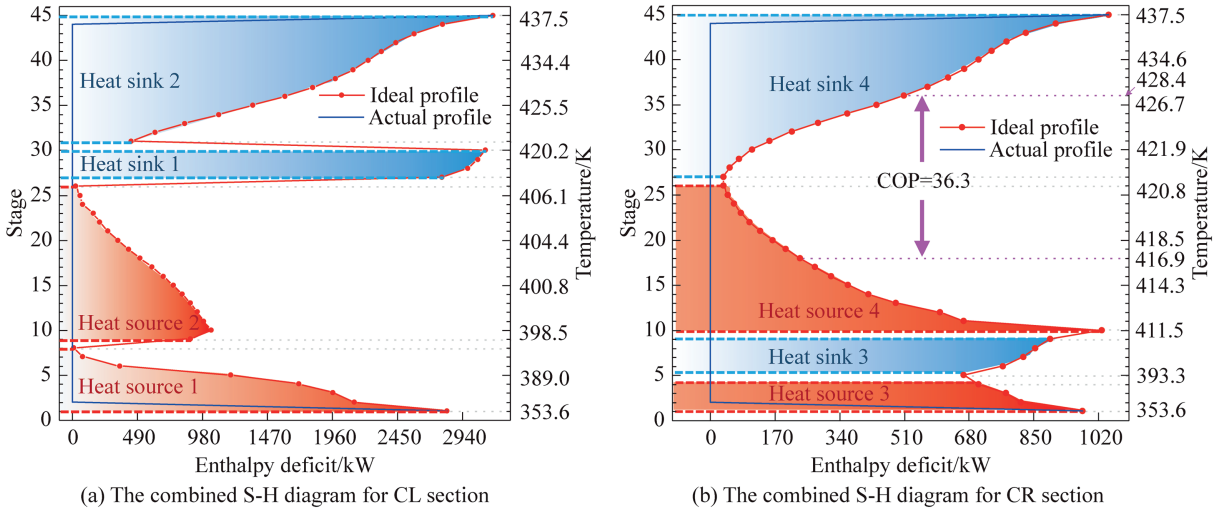

(a) The combined S-H diagram for CL section (b) The combined S-H diagram for CR section

Fig. 7. The combined S-H diagrams for LDWC separating the BzXM mixture.

nearly equal enthalpy deficit at the middle position of heat source 3 and heat sink 4, and because their COP is greater than 5 (calculated as 355.2/(400.5−355.2) = 7.8), the vapor stream can be extracted from heat source 3, compressed, and used to supply heat for heat sink 4. The bottom product can also be used to preheat the extracted steam to reduce compressor power. The intensified LDWC structure for the ESI = 1 system is illustrated in Fig. 5.

3.2.2. *Separation of the BzTM mixture with ESI<1*

For the BzTM (mesitylene (M)) system, the relative volatility between benzene and toluene is less than that between toluene and mesitylene, and ESI<1; the combined S-H diagrams of LDWC are shown in Fig. 6, and the stage temperatures are indicated on the right *y*-axis.

Fig. 6(a) shows the combined S-H diagram for the CL section, containing two potential heat sources and heat sinks. The heat sources span from stages 1 to 27, while the heat sinks span from stages 28 to 49. Similar to the LDWC separating the mixture with ESI = 1, modifying heat source 2 using VRC technology is not advisable due to the small enthalpy deficit and the high electric-thermal conversion coefficient. The enriched liquid needs to be extracted above heat sink 1 and sent to CR to improve column

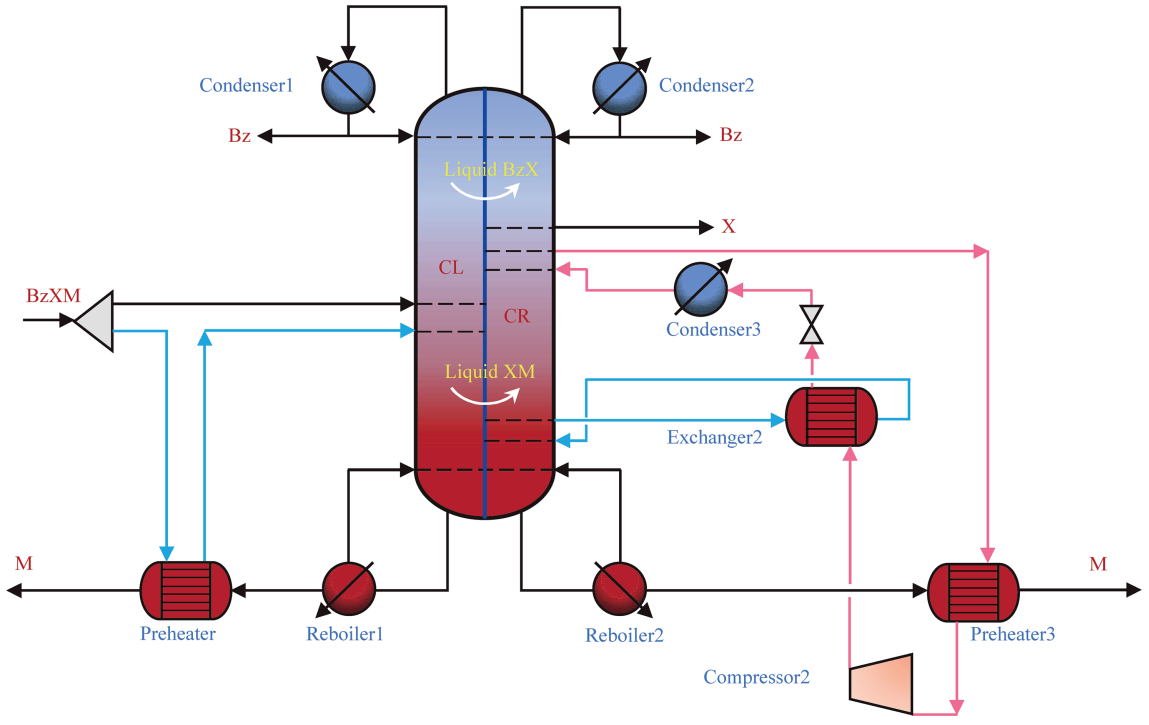

Fig. 8. Intensified LDWC structure for separating the BzXM mixture with ESI>1.

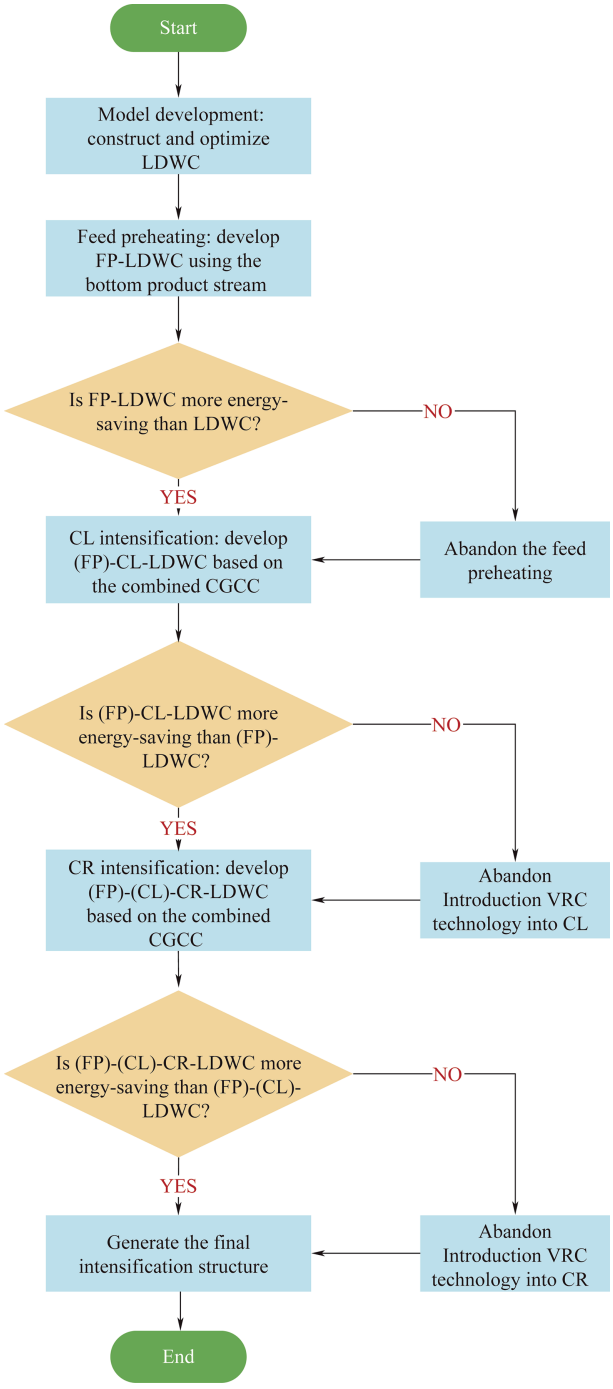

Fig. 9. The intensification strategy for LDWC.

operation. Modifying heat sink 1 using VRC technology could disrupt the material and energy balance of the column, leading to increased total energy consumption. Due to the high enthalpy deficit of heat source 1 and low enthalpy deficit of heat sink 2 in their middle position and their COP exceeds 5 (calculated as 363.5/(412.2−363.5) = 7.5), the vapor stream should be extracted from heat source 1, compressed by compressor, and used to provide heat for heat sink 2 through IR using VRC technology. The bottom product stream can also be used sequentially for partial feed vaporization and preheating the vapor stream.

Fig. 6(b) illustrates the combined S-H diagram for the CR section, containing two potential heat sources and heat sinks. The

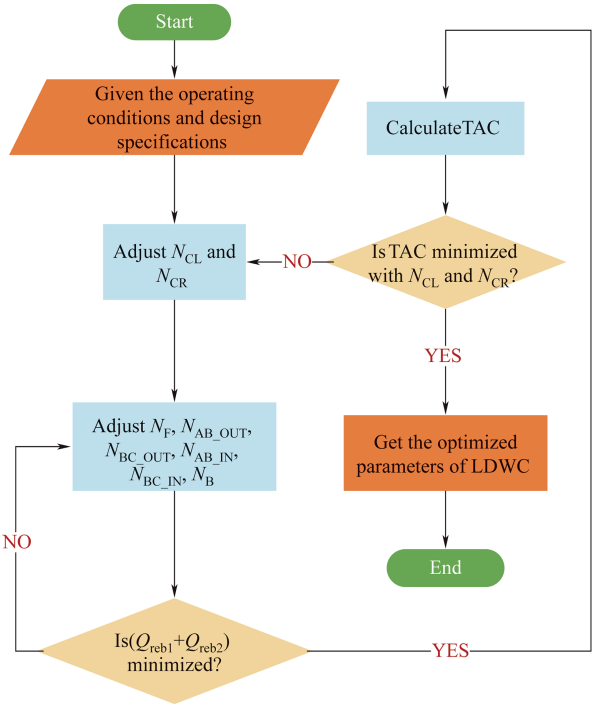

Fig. 10. Optimization model for LDWC.

heat sources are mainly distributed between stages 1 to 16 and stages 34 to 41, while the heat sinks are between stages 17 to 33 and stages 42 to 49. Similar to Fig. 5(b), extracting the vapor stream from heat source 4 and modifying heat sink 3 using VRC technology are not advisable; the vapor stream can be extracted from heat source 3, compressed, and used to provide heat for heat sink 4, because of the nearly equal enthalpy deficit at the middle position and their COP (calculated as 361.5/(411.0−361.5) = 7.3) is greater than 5. Additionally, using the bottom product stream to preheat the extracted vapor stream can reduce compressor power requirements. The intensified LDWC structure for the ESI<1 system is similar to those shown in Fig. 5, as illustrated in Fig. S2.

3.2.3. *Separation of the BzXM mixture with ESI>1*

For the BzXM system, the relative volatility between benzene and *p*-xylene is greater than that between *p*-xylene and mesitylene, and ESI>1. The combined S-H diagrams of the LDWC separating BzXM are shown in Fig. 7, and the stage temperatures are presented on the right y-axis.

Fig. 7(a) shows the combined S-H diagram for the CL section with two potential heat sources and heat sinks. The heat sources span from stages 1 to 26, while the heat sinks span from stages 27 to 45. The heat sink 1 is narrow, and modifying it using VRC technology could disrupt the material and energy balance within the column, increasing total energy consumption. The enthalpy deficit in heat source 2 is relatively small compared to that between the two heat sinks. If a vapor stream is extracted from heat source 2 and compressed to provide heat, the total energy consumption will increase due to excessive electricity consumption. The heat source 1 is narrow and near the top. Modifying heat source 1 using VRC technology will consume a large amount of electricity due to the wide temperature range between heat source 1 and sinks, which is caused by the high-boiling intermediate component *p*-xylene. Thus, modifying heat source 1 is impractical. The stream from the bottom can also be used to heat the feed, thereby utilizing energy effectively.

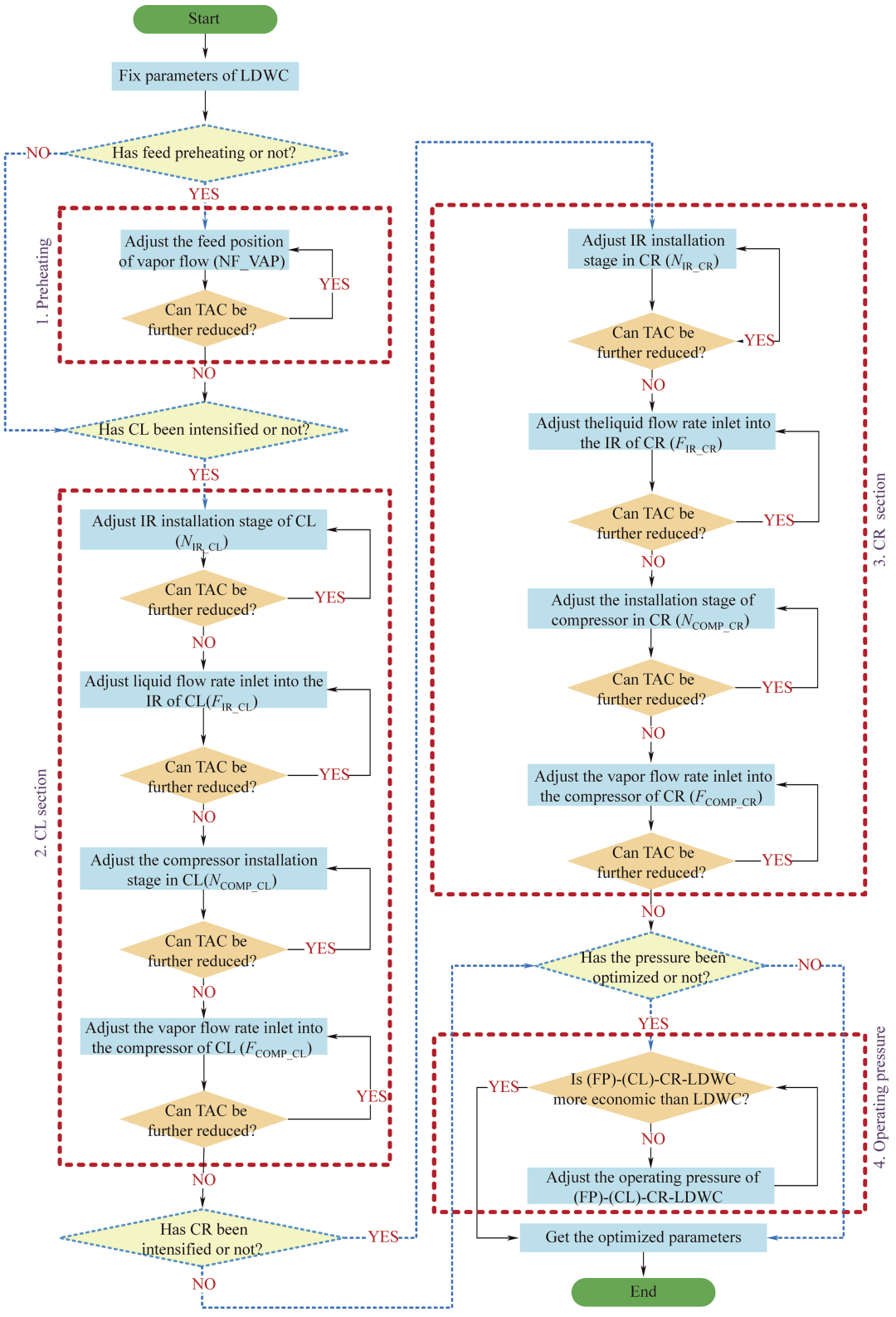

Fig. 11. Optimization model for intensified LDWC.

Fig. 7(b) shows the combined S-H diagram for the CR section. Two heat sources lie primarily between stages 1 to 4 and stages 10 to 26, while two heat sinks lie between stages 5 to 9 and stages 27 to 45. Different from the other two cases, heat source 3 and heat sink 3 are narrow and unsuitable for modification using VRC technology. Heat source 4 exhibits a significant heat deficit with a wide range, making it a viable candidate for vapor stream extraction and compression. This process can supply heat to the

Table 5
Optimized structural and independent process variables for LDWC and intensified LDWCs separating the BzTX mixture (ESI = 1).

	LDWC	FP-LDWC	FP-CL-LDWC	FP-CL-CR-LDWC1	FP-CL-CR-LDWC2
Operating pressure /kPa	101	101	101	101	61
RR_L	3.22	3.31	3.36	3.36	2.99
RR_R	2.64	2.67	2.70	1.56	1.48
N_{CL}	54	54	54	54	54
N_{CR}	54	54	54	54	54
N_F	26	26	26	26	26
N_{F_VAP}	–	28	28	28	28
N_{AB_OUT}	8	8	8	8	8
N_{BC_OUT}	37	37	37	37	37
N_{AB_IN}	9	9	9	9	9
N_{BC_IN}	37	37	37	37	37
N_B	20	20	20	20	20
N_{IR_CL}	–	–	42	42	42
N_{IR_CR}	–	–	–	43	43
N_{COMP_CL}	–	–	1	1	1
N_{COMP_CR}	–	–	–	4	4
F_{CLD}/kmol·h^{-1}	60.93	61.50	61.88	61.88	65.49
F_{CRD}/kmol·h^{-1}	38.84	38.26	37.89	37.80	34.39
F_{AB}/kmol·h^{-1}	83.37	83.37	83.37	83.37	81.59
F_{BC}/kmol·h^{-1}	89.14	89.14	89.14	89.14	89.14
F_B/kmol·h^{-1}	97.96	97.96	97.96	97.76	97.96
F_{IR_CL}/kmol·h^{-1}	–	–	50.00	50.00	50.00
F_{IR_CR}/kmol·h^{-1}	–	–	–	45.00	45.00
F_{COMP_CL}/kmol·h^{-1}	–	–	60.00	60.00	60.00
F_{COMP_CR}/kmol·h^{-1}	–	–	–	48.00	48.00

heat sink 4 through IR, and the COP at their middle exceeds 5 (calculated as 416.9/(428.4−416.9) = 36.3). The bottom stream can preheat the vapor stream to reduce compressor power further. The intensified LDWC for separating the BzXM mixture with ESI>1 is shown in Fig. 8.

3.3. The intensification strategy of LDWC

Based on the thermodynamic analysis and intensification design introduced in Section 3.2, a universal LDWC intensification strategy can be developed, as shown in Fig. 9. The details are as follows:

(1) **Model development**: an equivalent LDWC model for separating ternary mixtures is constructed and optimized by the built-in rigorous distillation module (RadFrac) in Aspen Plus.
(2) **Feed preheating**: the LDWC with preheated feed (FP-LDWC) is constructed to preheat the LDWC feed by the bottom product stream partially. It serves as the basis for further intensification if the total energy consumption of FP-LDWC is lower than that of the standard LDWC, which means performance improvement. However, the feed preheating will be abandoned if FP-LDWC's energy consumption is greater.
(3) **CL section intensification**: The thermal analysis indicates that the CL section presents potential heat sources and heat sinks. Therefore, it's possible to apply VRC technology in the intensification, which is named (FP)-CL-LDWC. It proceeds with further intensification if the total energy consumption of (FP)-CL-LDWC is lower than that of (FP)-LDWC; otherwise, abandon this step and move to the next step.
(4) **CR section intensification**: The CR section also presents potential heat sources and heat sinks. Utilizing VRC technology to build the structure (FP)-(CL)-CR-LDWC may be viable. If the total energy consumption of (FP)-(CL)-CR-LDWC is lower than that of (FP)-(CL)-LDWC, this intensification structure is viable; otherwise, it should be abandoned and moved to the next step.

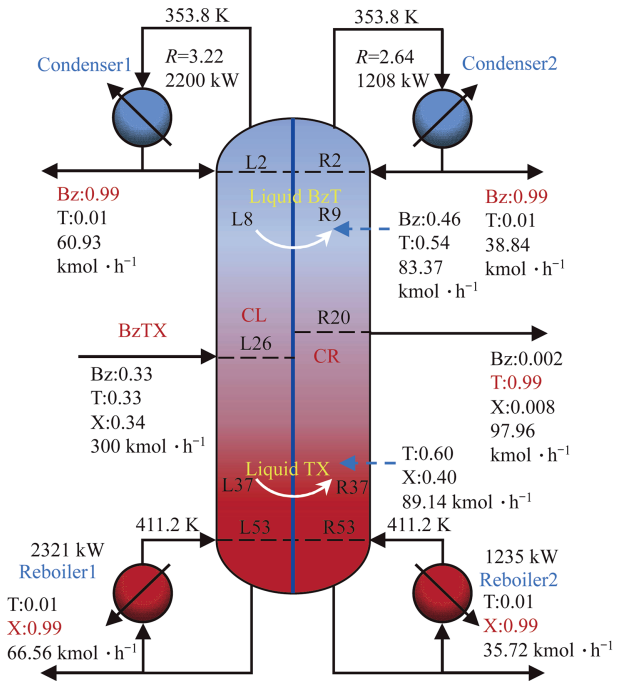

Fig. 12. The optimized results for LDWC separating the BzTX mixture (ESI = 1).

4. Process Optimization

The intensification of LDWCs can reduce energy consumption and increase equipment capital costs. Their structural and process

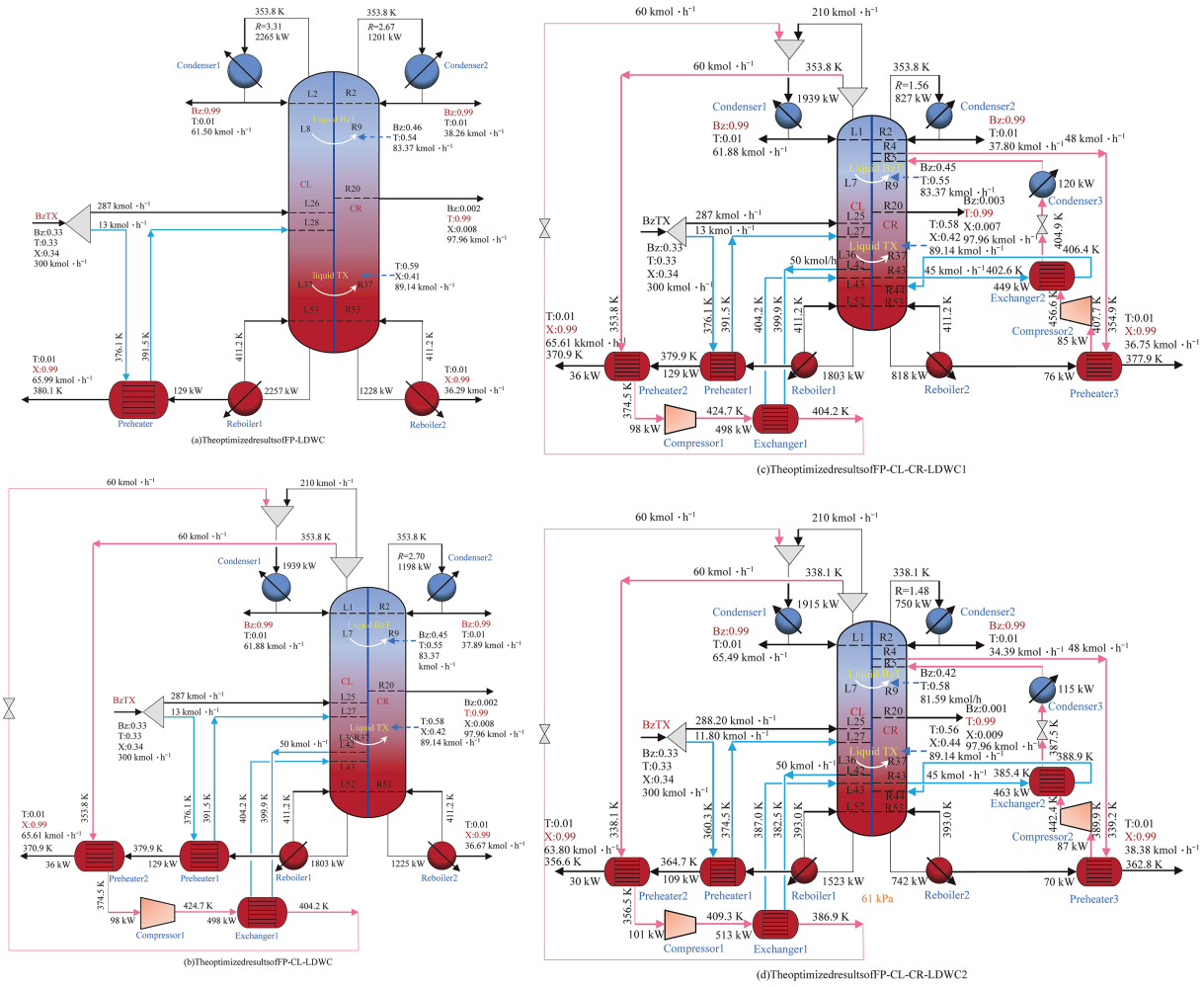

Fig. 13. The optimized results of intensified LDWCs separating the BzTX mixture (ESI = 1).

variables impact the distribution of enthalpy in CGCC, which in turn affects the process intensification of LDWC. Therefore, these variables should be optimized to balance energy consumption and equipment capital costs. The optimization model of LDWC and intensified LDWCs can be developed to minimize the TAC, which includes energy and capital costs using the sequential iterative approach. The base case's optimization model is illustrated in Fig. S3 in the supplementary material.

4.1. LDWC

For LDWC separating a ternary mixture, there are eight structural and seven independent process variables, as illustrated in Fig. 2. The eight structural variables include the theoretical stages of CL and CR (N_{CL}, N_{CR}), the feed position of CL (N_F), the extracted positions for liquid-only streams (N_{AB_OUT}, N_{BC_OUT}), the side product extracting position (N_B), and the feed positions for liquid-only streams into CR (N_{AB_IN}, N_{BC_IN}). The seven independent process variables are the reflux ratios for CL and CR (RR_L, RR_R), the distillate flow rates of CL and CR (F_{CLD}, F_{CRD}), the flow rates of liquid-only streams (F_{AB}, F_{BC}), and the side product flow rate (F_B).

Fig. 10 shows the LDWC optimization model. The product purity is maintained by manipulating the reflux ratios and product flow rates in Design Specifications and Vary modules, while F_{AB} and F_{BC} containing the specified substances are ensured by the Design Spec function. To facilitate industrial application and reduce installation complexity, the numbers of theoretical stages on both sides of the dividing wall (N_{CL} and N_{CR}) are assumed to be equal and are optimized first to minimize TAC.

Subsequently, the remaining structural variables (N_F, N_{AB_OUT}, N_{BC_OUT}, N_{AB_IN}, N_{BC_IN}, N_B) are sequentially adjusted in an upstream-to-downstream order to minimize the total reboiler duty ($Q_{reb1} + Q_{reb2}$). This specific optimization sequence is adopted because upstream variables significantly influence internal composition and energy distribution within the LDWC, thus impacting the optimization results of downstream variables. Moreover, following this sequential approach avoids redundant adjustments of downstream variables when changes occur upstream, thereby enhancing computational efficiency.

4.2. Intensified LDWC

Based on the LDWC intensification strategy, the optimization model involves feed preheating, CL section, and CR section. With the total number of stages on both sides of the LDWC, the positions of extracted side products, and the inlet and outlet positions of liquid-only streams specified, each intensified LDWC structure is optimized sequentially to investigate the impact of each intensification step on the LDWC. In addition, as the intensified LDWC increases capital cost (CC) due to the added compressors and heat

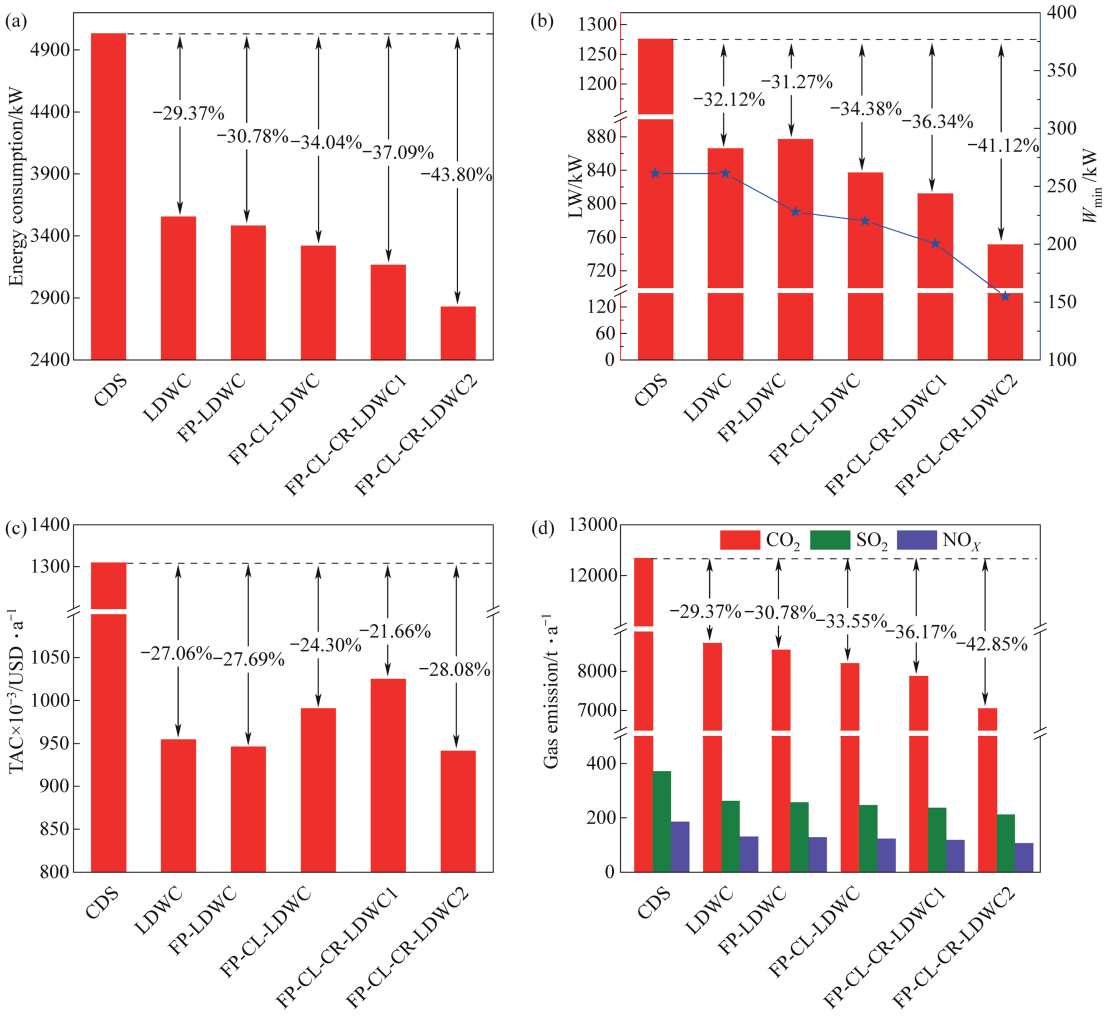

Fig. 14. Comparison of (a) total energy consumption, (b) W_{min} and LW, (c) TACs, and (d) gas emissions for all optimized systems separating the BzTX mixture (ESI = 1).

exchangers, the operating pressure is further optimized to balance CC and operating cost (OC), ensuring that the intensified and conventional LDWC configurations achieve similar TAC levels. This avoids the situation where differences in operating pressure dominate the TAC results, enabling a fair comparison of their thermodynamic efficiency and process performance under equivalent economic conditions.

An intensified LDWC optimization model consisting of four blocks is developed, as shown in Fig. 11.

(1) **Feed preheating optimization**: adjust the vapor feed position to minimize TAC continuously.
(2) O**ptimization of CL section**: adjust the installation position of the IR, the liquid flow rate entering the IR, the compressor installation position, and the vapor stream flow extracted from the CL section to minimize TAC.
(3) **Optimization of CR section**: similar to the optimization of CL section, adjust the corresponding variables to minimize TAC.

Table 6
The TACs of all optimized systems separating the BzTX mixture (ESI = 1).

	CDS	LDWC	FP-LDWC	FP-CL-LDWC	FP-CL-CR-LDWC1	FP-CL-CR-LDWC2
Capital cost (CC)/USD	1939456	1568451	1631939	2309507	2890254	2816141
Shell	1056343	840334	831054	826346	825934	867658
Tray	74885	63702	62682	62166	62121	66736
Heat exchanger	808227	664416	738203	907569	1033358	694918
Compressor	–	–	–	513426	968842	972232
CC saving (%)	0	19.13	15.86	−19.08	−49.02	−45.20
Operating cost (OC)/USD·a^{-1}	1115054	797883	783320	759955	736406	659775
Hot utilities	1065236	763143	747987	649736	562359	486185
Cold utilities	49818	34740	35333	31974	28200	27165
Electricity	–	–	–	78245	145847	146424
OC saving /%	0	28.44	29.75	31.85	33.96	40.83
TAC/USD·a^{-1}	1308999	954728	946514	990906	1025432	941389
TAC saving /%	0	27.06	27.69	24.30	21.66	28.08

Table 7
Optimized structural and independent process variables for LDWC and intensified LDWCs separating the BzTM mixture (ESI<1).

	LDWC	FP-LDWC	FP-CR-LDWC	FP-CL-CR-LDWC1	FP-CL-CR-LDWC2
Operating pressure /kPa	101	101	101	101	71
RR_L	1.86	1.98	1.47	1.47	1.41
RR_R	1.87	1.99	2.01	1.02	0.90
N_{CL}	49	49	49	49	49
N_{CR}	49	49	49	49	49
N_F	28	28	28	28	28
N_{F_VAP}	–	31	31	31	31
N_{AB_OUT}	17	17	17	17	17
N_{BC_OUT}	40	40	40	40	40
N_{AB_IN}	17	17	17	17	17
N_{BC_IN}	43	43	43	43	43
N_B	35	35	35	35	35
N_{IR_CL}	–	–	42	42	42
N_{IR_CR}	–	–	–	44	44
N_{COMP_CL}	–	–	8	8	8
N_{COMP_CR}	–	–	–	7	7
F_{CLD}/kmol·h^{-1}	68.98	70.62	70.88	70.88	72.17
F_{CRD}/kmol·h^{-1}	30.27	28.54	28.27	28.71	27.45
F_{AB}/kmol·h^{-1}	79.11	79.11	79.11	79.11	79.11
F_{BC}/kmol·h^{-1}	77.15	77.15	77.15	77.15	77.15
F_B/kmol·h^{-1}	97.96	97.96	97.96	97.96	97.96
F_{IR_CL}/kmol·h^{-1}	–	–	29.00	29.00	29.00
F_{IR_CR}/kmol·h^{-1}	–	–	–	27.00	27.00
F_{COMP_CL}/kmol·h^{-1}	–	–	39.00	39.00	39.00
F_{COMP_CR}/kmol·h^{-1}	–	–	–	30.00	30.00

(4) **Optimization of operating pressure**: adjust the operating pressure on both sides until the TAC is less than that of LDWC.

5. Results and Discussion

Applying the proposed process optimization models, the structural and independent process variables of the CDS, LDWC, and intensified LDWCs for different ESI systems are optimized to minimize TAC. Their performances are evaluated based on energy, exergy, economic, and environmental analysis.

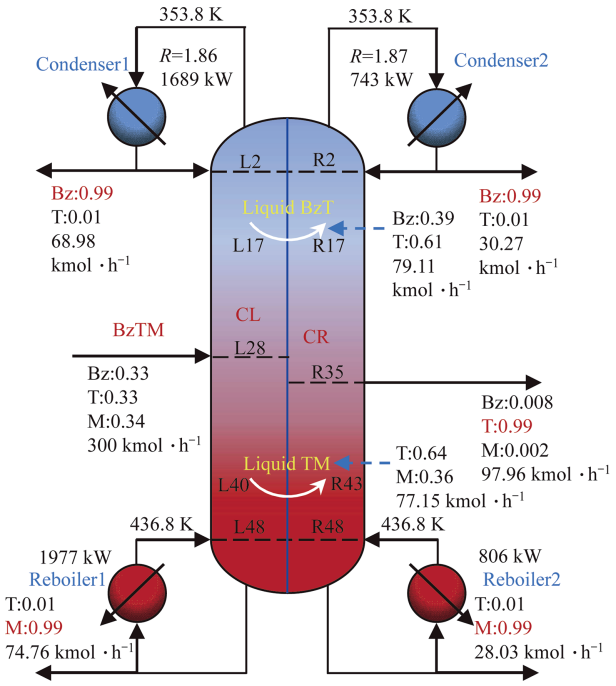

Fig. 15. The optimized results for LDWC separating the BzTM mixture (ESI<1).

5.1. The intensified LDWC separating the BzTX mixture with ESI = 1

For the separation of the BzTX mixture (ESI = 1), the optimized values of the structural and independent process variables for the LDWC and its intensified structures are presented in Table 5. The vapor feed stage (N_{F_VAP}) of the mixture is close to N_F; N_{AB_IN} is near to N_{AB_OUT}; N_{BC_IN} is equal to N_{BC_OUT}. The installation stage of the compressor in the CL section (N_{COMP_CL}) is positioned above N_{AB_OUT} at the top; the IR installation stage in the CL section (N_{IR_CL}) is below the N_{BC_OUT}; the compressor installation stage for the CR section (N_{COMP_CR}) is above N_{AB_IN}; the IR installation stage in CR section (N_{IR_CR}) is below N_{BC_IN}, The liquid flow rates into the IR for both the CL section (F_{IR_CL}) and CR section (F_{IR_CR}) remain unchanged, as do the vapor flow rates entering the compressors for the CL section (F_{COMP_CL}) and CR section (F_{COMP_CR}).

For the LDWC and intensified LDWCs, including FP-LDWC, FP-CL-LDWC, FP-CL-CR-LDWC1, and FP-CL-CR-LDWC2, the influence of structural and independent process variables on TAC are plotted in Fig. S4 and Fig. S5 of Supplementary Material, respectively. The suitable variables are specified when TAC has the lowest value. Then, the optimized structures are identified and shown in Figs. 12 and 13, respectively. The reboilers consume 671 kPa steam for heating, while cooling water is used for condensing.

For the base case, the influence of theoretical stages on TAC and optimized structure are displayed in Figs. S6 and S7 of supplementary material, respectively. The condensers use cooling water for complete condensation, while the reboilers use steam at 451 kPa and 671 kPa for heating, respectively.

The total energy consumption of all optimized systems is compared in Fig. 14(a), with the detailed data summarized in Table S2. For the CDS, LDWC, and FP-LDWC, the total energy consumption equals their heat duty, as electrical consumption is not considered in this figure. When compared to CDS, the total energy consumptions of other systems is significantly lower: LDWC, FP-LDWC, FP-CL-LDWC, FP-CL-CR-LDWC1, and FP-CL-CR-LDWC2

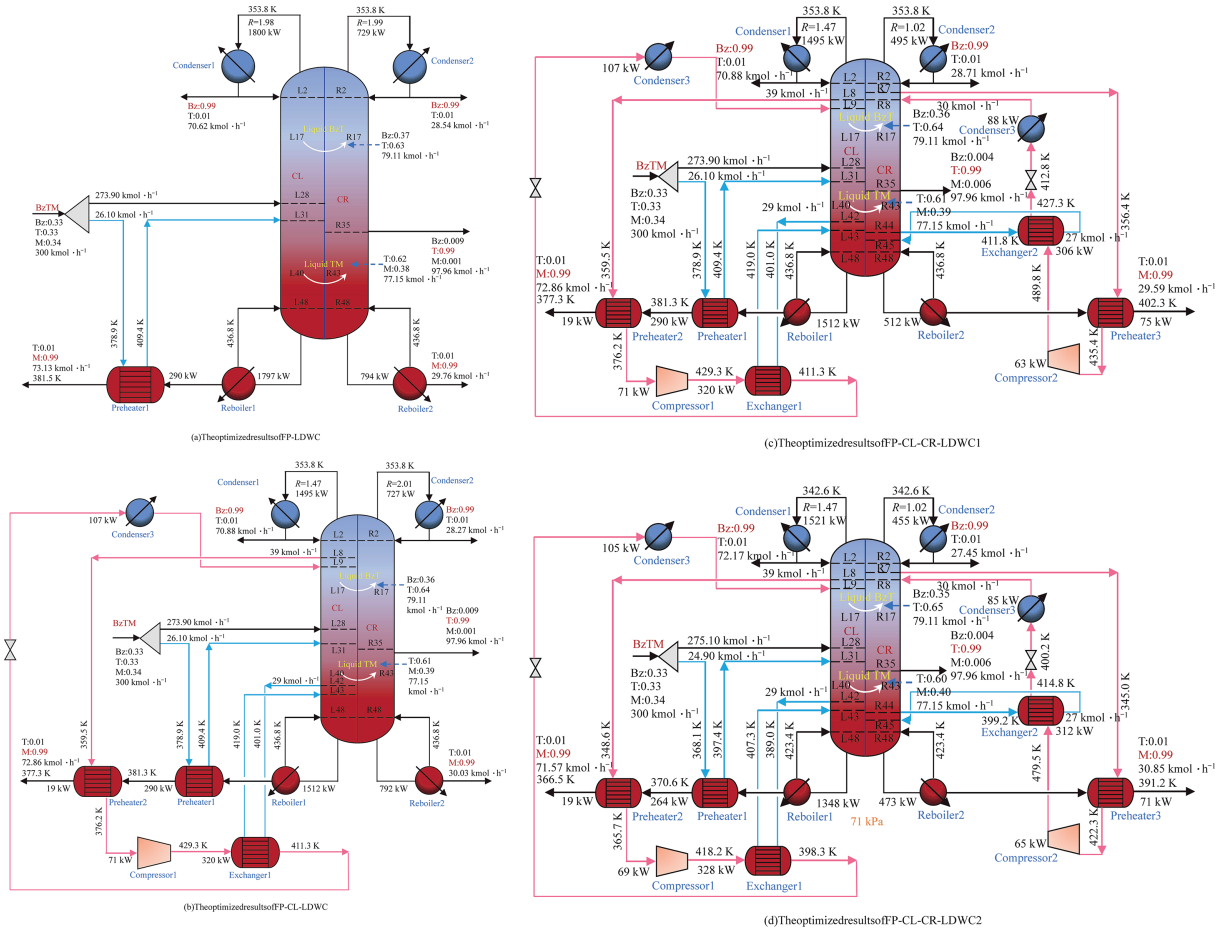

Fig. 16. The optimized results of intensified LDWCs separating the BzTM mixture (ESI<1).

show reductions of 29.37%, 30.78%, 34.04%, 37.09%, and 43.80%, respectively. Among these, the FP-CL-CR-LDWC2 exhibits the best performance, resulting in a reduction of total energy consumption from 5035 kW to 2830 kW.

W_{min} and LW of all optimized systems are compared in Fig. 14 (b), and the detailed data are listed in Table S3. CDS and LDWC have equal W_{min}. The utilization of the high-temperature heat of bottom streams can reduce W_{min}. Although FP-LDWC has a slightly higher LW than LDWC, it has a lower W_{min} and better energy performance. FP-CL-CR-LDWC2 exhibits the lowest W_{min} and LW.

TAC is mainly influenced by utility and electricity costs. The TACs of all optimized systems are compared in Fig. 14(c), and the detailed capital and operating costs are listed in Table 6. It can be seen that LDWC can save capital and operating costs compared to CDS, decreasing the TAC by 27.06%. Although the intensified LDWCs demand higher capital costs due to the expensive compressors and additional heat exchangers, the operating cost is reduced from 797883 USD·a^{-1} to 659775 USD·a^{-1}. The FP-CL-CR-LDWC2 yields the highest economic benefit, reducing TAC by 28.08% compared to CDS.

The gas emissions of all optimized systems are compared in Fig. 14 (d), and the details are provided in Table S4 in the supplementary material. It shows that gas emissions follow a similar trend as total energy consumption. The CDS has the

Table 8
TACs of all optimized systems separating the BzTM mixture (ESI<1).

	CDS	LDWC	FP-LDWC	FP-CL-LDWC	FP-CL-CR-LDWC1	FP-CL-CR-LDWC2
Capital cost (CC)/USD	1524996	1290128	1374024	1901103	2367464	2313209
Shell	772212	690169	663465	654974	646228	664105
Tray	47338	47927	45254	44415	43555	45318
Heat exchanger	705446	552033	665304	805154	922711	854637
Compressor	–	–	–	396560	754970	749149
CC saving (%)	0	15.40	9.90	−24.66	−55.24	−51.69
Operating cost (OC)/USD·a^{-1}	935445	654282	611804	601851	587508	540472
Hot utilities	896960	629493	586022	521007	457660	411850
Cold utilities	38485	24789	25781	23740	22268	22075
Electricity	–	–	–	57104	107581	106547
OC saving (%)	0	30.06	34.60	35.66	37.19	42.22
TAC/USD·a^{-1}	1087945	783294	749206	791961	824255	771793
TAC saving/%	0	28.00	31.14	27.21	24.24	29.06

Table 9
Optimized structural and independent process variables for LDWC and intensified LDWCs separating the BzXM mixture (ESI>1).

	LDWC	FP-LDWC	FP-CR-LDWC
Operating pressure/kPa	101	101	101
RR_L	3.05	3.23	3.23
RR_R	5.07	5.20	3.56
N_{CL}	45	45	45
N_{CR}	45	45	45
N_F	27	27	27
N_{F_VAP}	–	28	28
N_{AB_OUT}	5	5	5
N_{BC_OUT}	31	31	31
N_{AB_IN}	5	5	5
N_{BC_IN}	27	27	27
N_B	10	10	10
N_{IR_CR}	–	–	31
N_{COMP_CR}	–	–	12
F_{CLD}/kmol·h^{-1}	81.11	81.68	81.68
F_{CRD}/kmol·h^{-1}	18.72	18.15	17.92
F_{AB}/kmol·h^{-1}	79.91	79.91	79.91
F_{BC}/kmol·h^{-1}	64.55	64.55	64.55
F_B/kmol·h^{-1}	97.96	97.96	97.96
F_{IR_CR}/kmol·h^{-1}	–	–	30.00
F_{COMP_CR}/kmol·h^{-1}	–	–	33.00

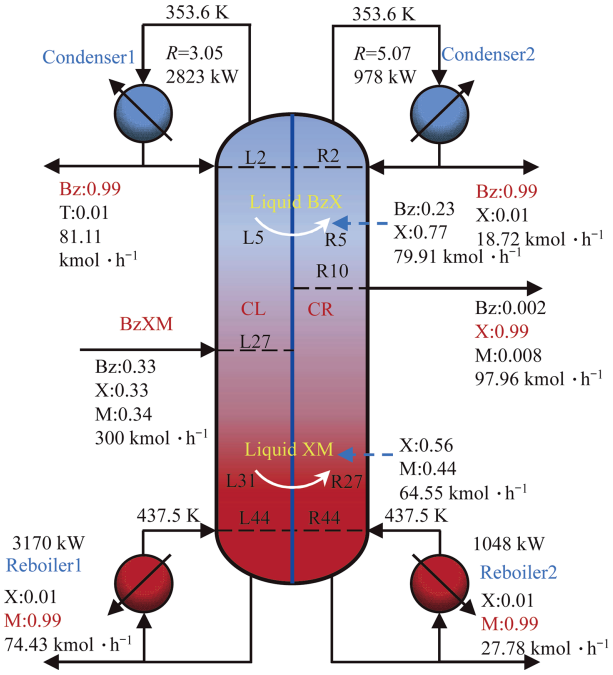

Fig. 17. The optimized results for LDWC separating the BzXM mixture (ESI>1).

poorest environmental performance due to the highest gas emissions. The LDWC and intensified LDWCs reduce gas emissions by 29.37%, 30.78%, 33.55%, 36.17%, and 42.85%, respectively, due to the reduction in total energy consumption. FP-CL-CR-LDWC2 exhibits the best environmental benefit, with the lowest total energy consumption, resulting in CO_2, SO_2, and NO_x emissions of 7050 t·a^{-1}, 212 t·a^{-1}, and 106 t·a^{-1}, respectively.

5.2. The intensified LDWC separating the BzTM mixture with ESI<1

For the LDWC and intensified LDWCs separating mixture (BzTM) with ESI<1, the optimized values of structural and independent parameters are illustrated in Table 7. The N_{F_VAP} is also near N_F; N_{AB_IN} is equal to N_{AB_OUT}; N_{BC_IN} is near to N_{BC_OUT}; N_{IR_CL}, N_{IR_CR}, N_{COMP_CL}, and N_{COMP_CR} have a similar relative position as those in the system separating the BzTX mixture (ESI = 1); F_{IR_CL}, F_{IR_CR}, F_{COMP_CL}, and F_{COMP_CR} are equal in the intensified LDWCs.

The impact of structural and independent process variables on TAC for the LDWC and intensified LDWCs are plotted in Figs. S8 and S9 of supplementary material, respectively. Optimal structures with the lowest TAC are specified and shown in Figs. 15 and 16. Meanwhile, 1221 kPa steam is used to heat the reboilers, and cooling water is employed to condense the vapor streams.

The impact of theoretical stages on TAC and optimized structure for the base case are displayed in Figs. S10 and S11, respectively. Cooling water and steam at 541 kPa and 1221 kPa are employed to condense the vapor streams and heat the reboilers, respectively.

The total energy consumptions are compared in Fig. S16(a), and the details are illustrated in Table S5. Compared to CDS, the total energy consumption of LDWC, FP-LDWC, FP-CL-LDWC, FP-CL-CR-LDWC1, and FP-CL-CR-LDWC2 are decreased by 32.56%, 37.22%, 38.99%, 41.19%, and 46.17%, respectively. The FP-CL-CR-LDWC2 performs best, reducing total energy consumption from 4126 kW to 2221 kW.

W_{min} and LW are compared in Fig. S16(b), with details illustrated in Table S6. The CDS and LDWC have equal W_{min}. Structures utilizing the high-temperature heat of bottom streams can reduce W_{min}. Besides, the LW of these systems is reduced compared to CDS. Although FP-LDWC has a slightly higher LW than LDWC, it has a lower W_{min} and, hence, improved performance. FP-CL-CR-LDWC2 has the lowest W_{min} and LW.

The TACs are compared in Fig. S16(c), with details in Table 8. Compared to CDS, LDWC has lower capital and operating costs, and its TAC has decreased by 27.06%. Although the intensified LDWCs require higher capital costs due to the compressors and additional exchangers, the operating cost is reduced from 654282 USD·a^{-1} to 540472 USD·a^{-1}. FP-CL-CR-LDWC2 performs best, with the TAC decreased by 29.06% compared to CDS.

The gas emissions are compared in Fig. S16(d). The CDS has the highest gas emissions and the poorest environmental performance. Compared to CDS, the LDWC and intensified LDWCs reduce gas emissions by 32.56%, 37.22%, 38.55%, 40.36%, and 45.35%, respectively, and this follows the same trend as the total energy consumption. FP-CL-CR-LDWC2 has the best environmental benefit, resulting in CO_2, SO_2, and NO_x emissions of 5525 t·a^{-1}, 166 t·a^{-1}, and 83 t·a^{-1}, respectively. The detailed gas emissions data are listed in Table S7.

5.3. The intensified LDWC separating the BzXM mixture with ESI>1

For the separation of the BzXM mixture with ESI>1, the optimized structural and independent process variables' values of the LDWC and their intensified structures, including FP-LDWC and FP-CR-LDWC, are listed in Table 9. N_{F_VAP} lies below N_F; N_{AB_IN} is equal to N_{AB_OUT}; N_{BC_IN} and N_{BC_OUT} are neighboring; different from separating the BzTX mixture (ESI = 1) and BzTM mixture (ESI<1), N_{COMP_CR} is below N_{AB_IN}; N_{IR_CR} lies below the N_{BC_IN} for FP-CR-LDWC.

The effect of structural and independent process variables on TAC for the LDWC and intensified LDWCs are illustrated in Figs. S12 and S13, respectively. The optimized structures with the lowest TAC value are illustrated in Figs. 17 and 18. Steam at 1231 kPa and cooling water are utilized to heat the reboilers and condense the overhead vapor, respectively. The effect of theoretical stages on TAC and optimized structure for the base case are illustrated in Figs. S14 and S15, respectively.

The total energy consumptions are compared in Fig. 19(a). Compared to CDS, the total energy consumption of LDWC, FP-LDWC, and FP-CR-LDWC decrease by 15.57%, 17.95%, and 21.64%, respectively. The FP-CR-LDWC performs best, reducing total

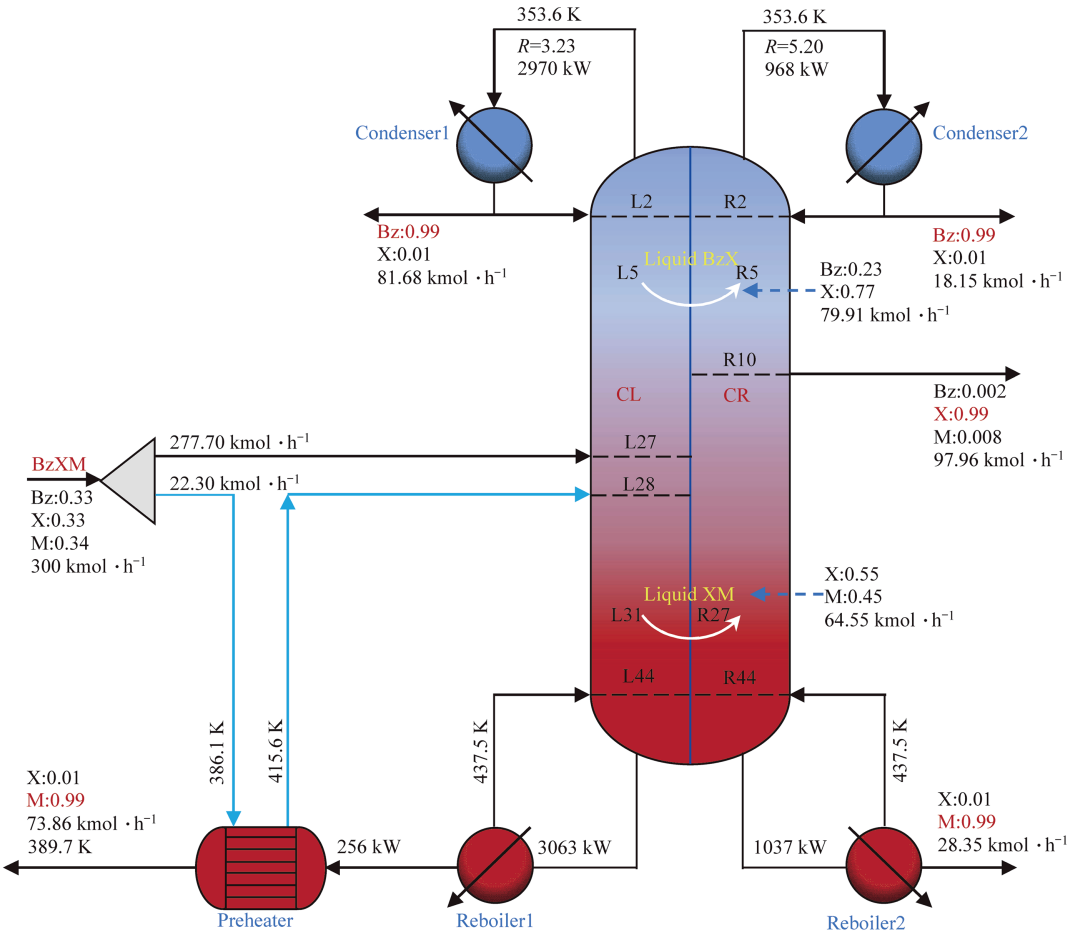

(a)TheoptimizedresultsofFP-LDWC

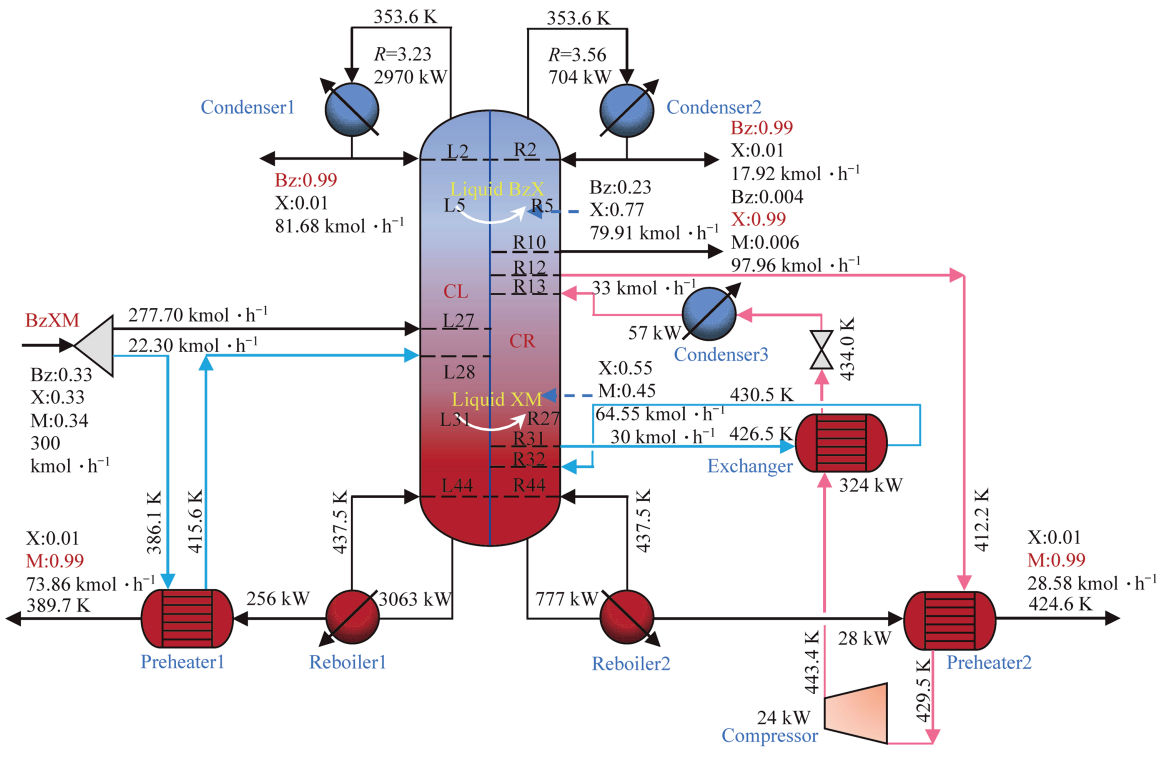

(b)TheoptimizedresultsofFP-CR-LDWC

Fig. 18. The optimized results of intensified LDWCs separating the BzXM mixture (ESI>1).

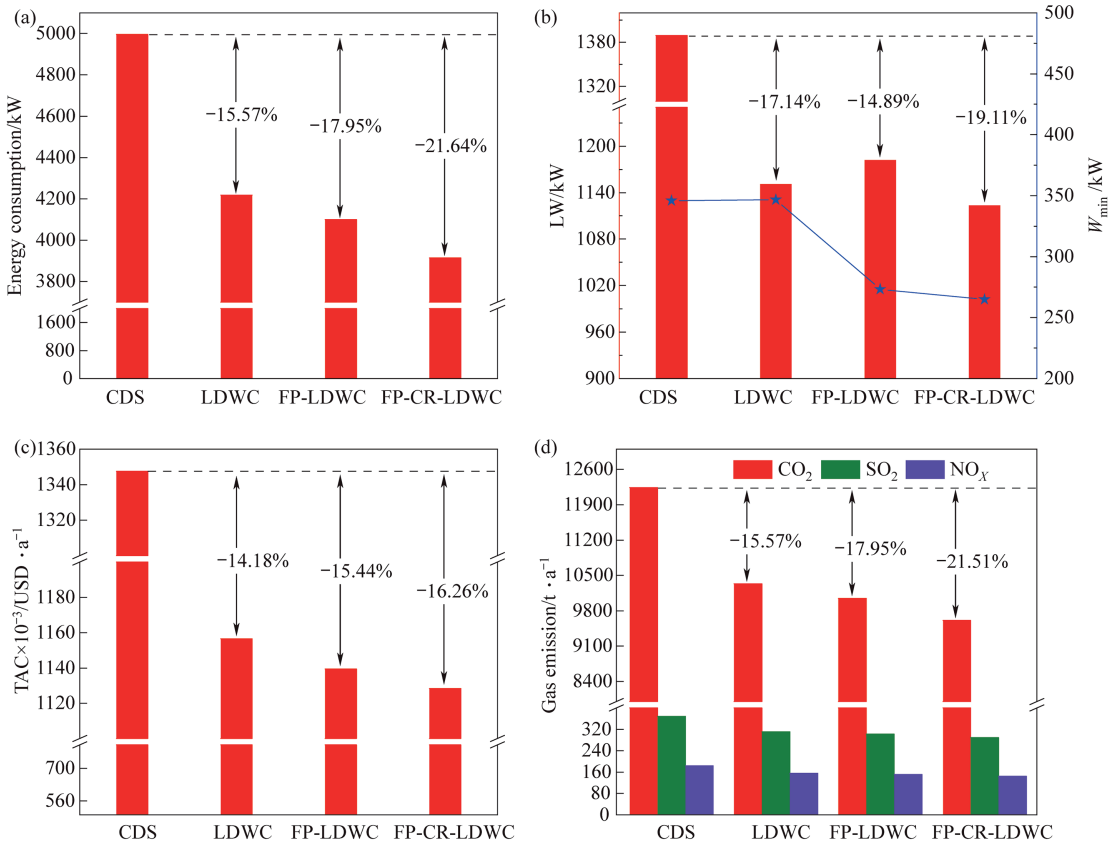

Fig. 19. Comparison of (a) total energy consumption, (b) W_{min} and LW, (c) TACs, and (d) gas emissions for all optimized systems separating the BzXM mixture (ESI>1).

Table 10
TACs of all optimized systems separating the BzXM mixture (ESI>1).

	CDS	LDWC	FP-LDWC	FP-CR-LDWC
Capital cost (CC)/USD	1824814	1628342	1712746	2014785
Shell	985242	825710	812623	815464
Tray	70571	62228	60799	61109
Heat exchanger	769000	740404	839323	973231
Compressor	–	–	–	164981
CC saving/%	0	10.77	6.14	−10.41
Operating cost (OC)/ USD·a^{-1}	1165114	993729	968199	926947
Hot utilities	1118405	954977	928053	869319
Cold utilities	46709	38752	40146	38032
Electricity	–	–	–	19597
OC saving/%	0	14.71	16.90	20.44
TAC/USD·a^{-1}	1347595	1156563	1139474	1128426
TAC saving/%	0	14.18	15.44	16.26

energy consumption from 4996 kW to 3915 kW. The detailed data are shown in Table S8.

W_{min} and LW are compared in Fig. 19(b), with details in Table S9. CDS and LDWC have equal W_{min}. The streams' molar entropy and enthalpy of FP-LDWC and FP-CR-LDWC are changed, reducing W_{min}. Besides, the LW of these structures has varying degrees of reduction compared to CDS. FP-LDWC has better operational performance than the LDWC due to its lower W_{min}. FP-CR-LDWC presents the best performance and the lowest W_{min} and LW.

The TACs are compared in Fig. 19 (c), with details illustrated in Table 10. LDWC saves capital and operating costs, with a TAC decrease of 14.18% compared to the CDS. Although FP-LDWC and FP-CR-LDWC demand higher capital costs, their operating costs decrease from 993729 USD·a^{-1} to 968199 USD·a^{-1} and 926947 USD·a^{-1}, respectively. FP- CR-LDWC performs best, and its TAC decreases by 16.26% compared to CDS.

The gas emissions are compared in Fig. 19 (d), and the details are listed in Table S10. The CDS has the highest gas emissions and the poorest environmental performance. Compared to CDS, the LDWC and intensified LDWCs' gas emissions are reduced by 15.57%, 17.95%, and 21.51%, respectively, which follows the same trend as total energy consumption. FP-CR-LDWC has the best environmental benefit, with CO_2, SO_2, and NO_X emissions of 9606 t·a^{-1}, 289 t·a^{-1}, and 145 t·a^{-1}, respectively.

6. Conclusions

A novel effective intensification strategy is proposed for the entire LDWC system to enhance energy efficiency based on the

combined column ground composite curve (CGCC). An optimization model, including four blocks, is developed to trade off the energy and capital costs of intensified LDWCs. Based on the proposed intensification strategy and optimization model, the intensified structures with optimal variables can be efficiently identified for the equimolar aromatic mixtures with different ESIs. Although the proposed intensification strategy was developed for equimolar aromatic mixtures, it can also be applied to systems separating ternary mixtures with non-equimolar feed, as they have the same LDWC structure. Its intensification structure depends on the distribution of potential heat sources/sinks.

For the separation of illustrative ternary mixtures, the intensified structures are identified. For the separation of equimolar BzTX mixtures (ESI = 1) and equimolar BzTM mixtures (ESI<1), the FP-CL-CR-LDWC2 configuration—featuring partial feed preheating, CL and CR section modification, and optimized operating pressure—has the lowest LW and W_{min}. Compared to CDS, its total energy consumption, TAC, and gas emissions are reduced by 43.80%, 28.08%, and 42.85% for the equimolar BzTX system, and by 46.17%, 29.06%, and 45.35% for the equimolar BzTM system. For the separation of equimolar BzXM mixture (ESI>1), the FP-CR-LDWC configuration—featuring partial feed preheating and CR modification—has the lowest LW and W_{min}. It achieves a significant reduction in total energy consumption, TAC, and gas emissions of 21.64%, 16.26%, and 21.51%, respectively.

While the proposed intensified strategy efficiently identifies high-performance intensified LDWC structures, it's important to note that this work focuses solely on separating ternary mixtures. The separation of multicomponent mixtures is a more complex task and will be the subject of our future work. Additionally, advanced algorithms will be incorporated into the optimization model to reduce calculation time further.

CRediT Authorship Contribution Statement

Zhongwen Song: Writing – original draft, Visualization, Software, Methodology, Investigation, Conceptualization. Chenghao Xing: Visualization, Validation, Software, Conceptualization. Yanyang Wu: Writing – review & editing, Supervision, Resources, Methodology, Conceptualization. Guilian Liu: Writing – review & editing, Supervision, Methodology, Data curation.

Declaration of Competing Interest

The authors declare the following financial interests/personal relationships which may be considered as potential competing interests: Guilian Liu reports financial support was provided by National Natural Science Foundation of China. If there are other authors, they declare that they have no known competing financial interests or personal relationships that could have appeared to influence the work reported in this paper.

Acknowledgements

Financial support provided by the National Natural Science Foundation of China (U24B6016) and the Higher Education Institution Academic Discipline Innovation and Talent Introduction Plan (“111 Plan”) (No. B23025) are gratefully acknowledged.

Nomenclature

A	light component
a	the conversion factors of equivalent coal, $kg \cdot kg^{-1}$
B	intermediate component
b	the conversion factors of electricity, $kg \cdot kW^{-1} \cdot h^{-1}$
C	heavy component
CC	capital cost, USD
c	the conversion coefficient of electricity to heat
F_{CLD}	distillate flow rate of CL, $kmol \cdot h^{-1}$
F_{CRD}	distillate flow rate of CR, $kmol \cdot h^{-1}$
F_{AB}	flow rate of stream AB, $kmol \cdot h^{-1}$
F_{BC}	flow rate of stream BC, $kmol \cdot h^{-1}$
F_{B}	flow rate of side product, $kmol \cdot h^{-1}$
F_{IR_CL}	liquid flow rate into IR of CL, $kmol \cdot h^{-1}$
F_{IR_CR}	liquid flow rate into IR of CR, $kmol \cdot h^{-1}$
F_{COMP_CL}	vapor flow rate into compressor of CL, $kmol \cdot h^{-1}$
F_{COMP_CR}	vapor flow rate into compressor of CR, $kmol \cdot h^{-1}$
H	molar enthalpy, $kmol \cdot h^{-1}$
LW	lost work, kW
M&S	marshall & Swift index
M_{coal}	equivalent coal, $t \cdot a^{-1}$
m	molar flow rate, $kmol \cdot h^{-1}$
N_{CL}	theoretical stages of CL
N_{CR}	theoretical stages of CR
N_{F}	liquid mixture's feed position of CL
N_{F_VAP}	vapor mixture's feed position of CL
N_{AB_OUT}	liquid-only transfer stream AB's extracted position
N_{BC_OUT}	liquid-only transfer stream BC's extracted position
N_{AB_IN}	liquid-only transfer stream AB's feed position
N_{BC_IN}	liquid-only transfer stream BC's feed position
N_{B}	side product's extracted position
N_{IR_CL}	IR installation stage of CL
N_{IR_CR}	IR installation stage of CR
N_{COMP_CL}	compressor installation stage of CL
N_{COMP_CR}	compressor installation stage of CR
OC	operating cost, $USD \cdot a^{-1}$
Q	the heat duty of the reboiler or condenser, kW
Q_{E}	total energy consumption, kW
RR_{L}	reflux ratio of CL
RR_{R}	reflux ratio of CR
Q_{R}	the sum of all heater's heat duty, kW
Q_{reb1}	heat duty of reboiler1, kW
Q_{reb2}	heat duty of reboiler2, kW
S	molar entropy, $kmol \cdot h^{-1}$
T	the temperature of the heat source or sink, K
TAC	total annual cost, $USD \cdot a^{-1}$
T_0	environment temperature, K
W_{elec}	the electricity consumption, $kW \cdot h \cdot a^{-1}$
W_{in}	the work done to the system by pumps, kW
W_{min}	minimum work, kW
W_{n}	the electricity requirement of units, kW
W_{out}	the work done to the surrounding by turbines, kW

Subscripts

i	The type of gas
in	Inlet of the system
out	Outlet of the system

Supplementary Material

Supplementary data to this article can be found online at https://doi.org/10.1016/j.cjche.2025.07.021.

References

[1] L. Zhao, G. Liu, Optimization of catalyst service cycle and start-up considering the reactor-distillation-HEN integration and climate, *Chem. Eng. Sci.* 299 (2024) 120517.
[2] S. David S, R.P. Lively, Seven chemical separations to change the world, *Nature* 532 (2016) 435–437.

[3] A.A. Kiss, R. Smith, Rethinking energy use in distillation processes for a more sustainable chemical industry, *Energy* 203 (2020) 117788.
[4] Y.J. Lee, H.Y. Jang, B.D. Marshall, M.I.L. Abutaqiya, N. Rangnekar, N.C. Bruno, M.G. Finn, R.P. Lively, Fractionation of complex aromatic hydrocarbon mixtures using membrane cascades hybridized with distillation, *Chem. Eng. J.* 503 (2025) 158170.
[5] D. Liu, Y. Sun, W. Li, X. Cai, G. Zhang, Y. Huang, R. Wei, Z. Zhang, J. Tang, X. Qiao, A novel integration of reaction distillation and pervaporation membrane for producing n-propyl propionate, *Chem. Eng. Res. Des.* 204 (2024) 330–342.
[6] A.S. Horsch, M. Skiborowski, Thermally coupled distillation columns without vapor transfer – current state and further needs, *Sep. Purif. Technol.* 354 (2025) 128762.
[7] R. Agrawal, Thermally coupled distillation with reduced number of intercolumn vapor transfers, *AIChE J.* 46 (2000) 2198–2210.
[8] R.O. Wright, Fractionation apparatus, US Patent 2471134(1949).
[9] G. Kaibel, Distillation columns with vertical partitions, *Chem. Eng. Technol.* 10 (1987) 92–98.
[10] B. Kolbe, S. Wenzel, Novel distillation concepts using one-shell columns, *Chem. Eng. Process. Process Intensif.* 43 (2004) 339–346.
[11] L.T. Maralani, X. Yuan, Y. Luo, C. Gong, G. Yu, Numerical investigation on effect of vapor split ratio to performance and operability for dividing wall column, *Chin. J. Chem. Eng.* 21 (2013) 72–78.
[12] G.M. Ramapriya, M. Tawarmalani, R. Agrawal, Thermal coupling links to liquid-only transfer streams: a path for new dividing wall columns, *AIChE J.* 60 (2014) 2949–2961.
[13] Z. Jiang, G. Madenoor Ramapriya, M. Tawarmalani, R. Agrawal, Minimum energy of multicomponent distillation systems using minimum additional heat and mass integration sections, *AIChE J.* 64 (2018) 3410–3418.
[14] R. Watzdorf, J. Bausa, W. Marquardt, Shortcut methods for nonideal multicomponent distillation: 2. Complex columns, *AIChE J.* 45 (1999) 1615–1628.
[15] Z. Feng, W. Wang, D. Xu, G.P. Rangaiah, L. Dong, Dynamic controllability of temperature difference control for the operation of double liquid-only sidestream distillation, *Comput. Chem. Eng.* 164 (2022) 107870.
[16] T. Zhang, M. Li, H. Pan, H. Ling, Dynamic control of liquid-only transfer kaibel dividing-wall column, *Chem. Eng. Sci.* 272 (2023) 118589.
[17] Y. Wu, Z. Song, J. Rao, Y. Yao, B. Wu, K. Chen, L. Ji, Separation of ternary system 1,2-ethanediol + 1,3-propanediol + 1,4-butanediol by liquid-only transfer dividing wall column, *Processes* 11 (2023) 3150.
[18] C. Cui, X. Zhang, J. Sun, Design and optimization of energy-efficient liquid-only side-stream distillation configurations using a stochastic algorithm, *Chem. Eng. Res. Des.* 145 (2019) 48–52.
[19] C. Cui, Q. Zhang, X. Zhang, J. Sun, Eliminating the vapor split in dividing wall columns through controllable double liquid-only side-stream distillation configuration, *Sep. Purif. Technol.* 242 (2020) 116837.
[20] B. Liu, T. Zhang, Y. Zheng, K. Li, H. Pan, H. Ling, A dynamic control structure of liquid-only transfer stream distillation column, *Chin. J. Chem. Eng.* 59 (2023) 135–145.
[21] B. Kong, Q. Zhang, C. Cui, J. Sun, Optimal design and effective control of kaibel column with liquid-only transfer streams for quaternary distillation, *Sep. Purif. Technol.* 250 (2020) 117261.
[22] Y. Li, G. Li, J. Zhao, T. Zhang, Z. Wang, H. Pan, H. Ling, Dynamic control of liquid-only transfer stream agrawal divided-wall column, *Ind. Eng. Chem. Res.* 62 (2023) 18579–18590.
[23] Z. Song, W. Cui, Y. Wu, B. Wu, K. Chen, L. Ji, Energy, exergy, economic, and environmental analysis of a novel liquid-only transfer dividing wall column with vapor recompression, *Sep. Purif. Technol.* 329 (2024) 125122.
[24] L. Xu, M. Li, X. Ge, X. Yuan, Numerical simulation of dividing wall column with vapor recompression located at side product stage, *Chem. Eng. Res. Des.* 120 (2017) 138–149.
[25] S. Tututi-Avila, N. Medina-Herrera, J. Hahn, A. Jiménez-Gutiérrez, Design of an energy-efficient side-stream extractive distillation system, *Comput. Chem. Eng.* 102 (2017) 17–25.
[26] C. Xing, Z. Song, Y. Wu, B. Wu, K. Chen, L. Ji, Energy, Exergy, Economic, and environmental analysis of the vapor recompression-assisted liquid-only transfer extractive dividing wall column for separating minimum-boiling point azeotropes, *Ind. Eng. Chem. Res.* 63 (15) (2024) 6725–6742.
[27] D.W. Tedder, D.F. Rudd, Parametric studies in industrial distillation: part I. Design comparisons, *AIChE J.* 24 (1978) 303–315.
[28] F. Zhou, L. Zhong, C. Chen, Y. Li, C. Xu, Isobaric vapor–liquid equilibrium for binary and ternary systems of isoamyl alcohol + isoamyl acetate + dimethyl sulfoxide at 101.33 kPa, *J. Chem. Eng. Data* 62 (2017) 691–697.
[29] A. Hu, K. Liu, Z. Jin, Vapor-liquid equilibrium data for toluene - *p*-xylene, *Shiyou Huagong* 5 (1990) 28–30.
[30] Z. Jin, A. Hu, K. Liu, Vapor-liquid equilibrium of binary and ternary systems comprising benzene, toluene and p-xylene, *Huaxue Gongcheng* 5 (1991) 56–60. (in Chinese)
[31] H. Renon, J.M. Prausnitz, Local compositions in thermodynamic excess functions for liquid mixtures, *AIChE J.* 14 (1968) 135–144.
[32] D.S. Abrams, J.M. Prausnitz, Statistical thermodynamics of liquid mixtures: a new expression for the excess Gibbs energy of partly or completely miscible systems, *AIChE J.* 21 (1975) 116–128.
[33] K. Iwakabe, M. Nakaiwa, K. Huang, T. Nakanishi, A. Røsjorde, T. Ohmori, A.T. Yamamoto, Energy saving in multicomponent separation using an internally heat-integrated distillation column (HIDiC), *Appl. Therm. Eng.* 26 (2006) 1362–1368.
[34] A.K. Jana, A. Mane, Heat pump assisted reactive distillation: wide boiling mixture, *AIChE J.* 57 (2011) 3233–3237.
[35] D. Favrat, M. Kane, Exergy and industrial processes, in: Exergy Anal. Heat. Cool., Elsevier, 2025, pp. 299–368.
[36] S. Zhang, G. Liu, Thermal design and performance optimization of the four-step Cu–Cl cycle coupled with clean energy for hydrogen production, *J. Clean. Prod.* 422 (2023) 138593.
[37] W.D. Seider, D.R. Lewin, J.D. Seader, S. Widagdo, R. Gani, K.M. Ng, Product and Process Design Principles: Synthesis, Analysis, and Evaluation, fourth ed., John Wiley & Sons Inc., New York, 2017.
[38] J.M. Douglas, Conceptual Design of Chemical Processes, McGraw-Hill, New York, 1988.
[39] W.L. Luyben (Ed.), Distillation Design and Control Using Aspen™ Simulation, John Wiley & Sons, Inc., Hoboken, New Jersey, 2013.
[40] Z. Si, H. Chen, H. Cong, X. Li, Energy, exergy, economic and environmental analysis of a novel steam-driven vapor recompression and organic Rankine cycle intensified dividing wall column, *Sep. Purif. Technol.* 295 (2022) 121285.
[41] Q. Li, Z. Feng, G.P. Rangaiah, L. Dong, Process optimization of heat-integrated extractive dividing-wall columns for energy-saving separation of CO_2 and hydrocarbons, *Ind. Eng. Chem. Res.* 59 (2020) 11000–11011.
[42] C. Cui, X. Li, D. Guo, J. Sun, Towards energy efficient styrene distillation scheme: from grassroots design to retrofit, *Energy* 134 (2017) 193–205.
[43] Y. Hu, S. Naito, N. Kobayashi, M. Hasatani, CO_2, NO_x and SO_2 emissions from the combustion of coal with high oxygen concentration gases, *Fuel* 79 (2000) 1925–1932.
[44] H. Chen, X. Li, L. He, H. Cong, Energy, exergy, economic, and environmental analysis for methyl acetate hydrolysis process with heat integrated technology used, *Energy Convers. Manag.* 216 (2020) 112919.
[45] K. Huang, S. Han, L. Zang, H. Chen, Y. Luo, L. Zhang, Y. Yuan, X. Qian, S. Wang, Configuring topologically optimum vapor recompressed dividing-wall distillation columns to maximize operating efficiency, *Chin. J. Chem. Eng.* 57 (2023) 247–264.
[46] V.R. Dhole, B. Linnhoff, Distillation column targets, *Comput. Chem. Eng.* 17 (1993) 549–560.
[47] V. Pleşu, A.E. Ruiz, J. Bonet, J. Llorens, Simple equation for suitability of heat pump use in distillation, in: Comput. Aided Chem. Eng., Elsevier, 2014, pp. 1327–1332.